Ahmed Hussein, BSc.

Electron Beam Welding and Post Weld Heat Treatment of S960MC

to achieve the university degree of
Master of Science
Master's degree programme: Advanced Materials Science

submitted to

Graz University of Technology

Supervisor
Dipl.-Ing.Christian Schneider
Assoc.Prof. Dipl.-Ing. Dr.techn.Norbert Enzinger

IMAT-Institute of Materials Science, Joining and Forming
Head: Univ.-Prof. Dipl.-Ing. Dr.techn.Christof Sommitsch

Graz, June 2018

Abstract

Ultra high strength low alloy steels (UHSLA) are characterized by their good mechanical properties such as high strength with adequate toughness and excellent cost efficiency compared to conventional steels. It is possible to build thinner and lighter structures that can be used in a wide range of applications such as cranes, bridges or offshore structures. Welding of UHSLA steels is of great importance for their utilization as it influences the final mechanical properties as well as the total cost of the component.

Electron beam welding is a high energy fusion welding process which enables single pass welding of thick sheets, while obtaining a narrow weld zone. However, fast cooling leads to high peak hardness and unfavorable impact toughness of the joints. Current research is seeking to improve welding processes for UHSLA steels giving much consideration on improving the toughness properties in the weld zone.

In this study electron beam welding (EBW) is used to join 8 mm thick sheets of thermomechanically controlled processed (TMCP) UHSLA steel. Electron beam local post weld heat treatment (EBLPWHT) is implemented after the welding process. The EBLPWHT is achieved via a second "welding cycle" with lower beam power and reduced power density which enables the reheating of the weld seam directly or shortly after the welding process. The first welding cycle is used for the actual welding process and the second cycle for the local post weld heat treatment (LPWHT). The EBLPWHT sheets are compared to conventional electron beam welded sheets and post weld heat treated samples using the Gleeble. The microstructure is investigated using light optical- (LOM) and scanning electron microscopy (SEM). The mechanical properties are analyzed via impact-, tensile- and hardness tests.

Kurzfassung

Ultra-hochfeste Stähle spielen eine entscheidende Rolle im innovativen Leichtbau. Durch die höhere Festigkeit kann die Bauteildicke verringert und damit Gewicht eingespart werden. Die Einsatzgebiete reichen von Schienenfahrzeugen, Nutzfahrzeugen bis zu Mobilkränen. Die Schweißeignung stellt einen wichtigen Aspekt für die industrielle Nutzbarkeit dieser Materialien dar. Das Elektronenstrahlschweißen ist ein Schmelzschweißverfahren, welches dank seiner extrem hohen Energiedichte das Schweißen dickwandiger Bauteile mit einer einzigen Lage ermöglicht. Durch die hohe Abkühlrate treten allerdings lokale Härtespitzen in der Fügezone auf, die sich je nach Belastungsart, negativ auf die Zähigkeit der Schweißnähte auswirken können.

Die Forschung in der Schweißtechnik beschäftigt sich stark mit der Weiterentwicklung von Schweißverfahren für ultrahochfeste Stähle. Vor allem die finalen Zähigkeitseigenschaften der Schweißnaht sind von besonderem Interesse.

In dieser Arbeit wurden 8 mm dicke Bleche eines thermomechanisch gewalzten Stahls mittels Elektronenstrahlschweißen geschweißt und anschließend mit dem Elektronenstrahl lokal wärmenachbehandelt. Diese Wärmenachbehandlung funktioniert wie ein zweiter „Schweißzyklus“ mit geringerer Leistung, wodurch die Schweißnaht lokal wiedererwärmt wird. Die wärmenachbehandelten Bleche werden mit den geschweißten Referenzblechen verglichen. Die mechanischen Eigenschaften werden durch Zug-, Kerbschlagbiegeversuche und Härtetests ermittelt. Die Mikrostruktur wird mittels Lichtmikroskopie und Rasterelektronenmikroskopie untersucht.

Declaration

I declare that I have authored this thesis independently, that I have not used other than the declared sources/resources, and that I have explicitly indicated all material which has been quoted either literally or by content from the sources used. The text document uploaded to TUGRAZ online is identical to the present master‘s thesis.

Date	Signature

Acknowledgements

I would like to express my deep appreciation for those who helped me throughout my way to finish my thesis. Without their great assistance, engorgement and follow up, this work would not have been achieved.

I would first like to thank Christian Schneider, Assoc.Prof. Norbert Enzinger and everyone at the IMAT. Christian Schneider office was always open whenever I ran into a trouble spot or had a question about my research or writing.

Additionally Dr. Wolfgang Ernst and Voestalpine for sample preparation and their support.

The K-Project Network of Excellence for Metal JOINing is fostered in the frame of COMET – Competence Centers for Excellent Technologies by BMWFW, BMVIT, FFG, Land Oberösterreich, Land Steiermark, Land Tirol and SFG. The programme COMET is handled by FFG (Österreichische Forschungsförderungsgesellschaft).

Thanks extended also to my parents who always supported me during my studies. My brother and Norhan for providing me with unfailing support. I am also deeply thankful for my friends and colleagues who helped and supported me during my studies, especially Alain, Jasmine, Marlene, Omar and Sandro.

Contents

Chapter 1

Literature review

1.1 High strength and ultra high strength steels

Steel shows a great importance as a dominant alloy in many applications due to its wide range of properties, flexible manufacturing techniques and market demand, cost effectiveness in addition to it can be easily reused and recycled. Steel offers a wide range of properties that can be generated by many modifications such as alloying, solid state transformations and processing [1].

1.1.1 High strength steels

High strength steels (HSS) (yield strength higher than 275 MPa to 700 MPa [2] (see Figure 1) are optimized to achieve a range of properties depending on the application. High strength steel is more complex than conventional steels because the chemical composition, microstructure and heat treatment are selected precisely in order to achieve the high strength. Strengthening techniques are employed in order to achieve the desired range of properties such as toughness, ductility and strength [3].

HSS steel strength does not only depend on the carbon content and heat treatments compared to conventional steels. Instead HSS depends on other strengthening methods in order to obtain the desired properties depending on the application such as high strength with improved toughness and weldability [4, 5, 6]. The strengthening mechanisms are:

- Solid solution strengthening by substitution and interstitial elements such as Mn and Si.
- Precipitation strengthening.
- Grain refinement and transformation strengthening.
- Dislocation hardening .

1.1.2 Ultra high strength steels

Structural steels with very high strength levels are usually called ultra high strength steels (UHSS) [6] or Advanced High strength steels (AHSS) by the automotive industry. The UHSS yield strength is higher than 700 MPa, see Figure 1 [2]. The diagram shows the tensile strength and total elongation of the steels. The UHSS region shows different kinds of steels starting with the high strength low alloyed steel (HSLA) and dual phase and complex phase steel (DP-CP). Furthermore high manganese content steels transformation induced plasticity (TRIP) steel and twinning-Induced Plasticity steel (TWIP). Finally martensitic steels with the highest tensile strength [2].

Martensitic steels

Martensitic steels (MART) show high strengths up to 1700 MPa ultimate tensile strength. The microstructure of MART steel is characterized by a martensitic matrix which can contain small amounts of residual austenite, ferrite and/or bainite. MART is created by quenching the austenite that exists during hot-rolling or annealing, rapid cooling transforms almost all the austenitic structure to martensitic structure. Another method to develop martensitic steel is post forming heat treatment. Usually martensitic steels undergoes post quench tempering in order to improve the ductility [7].

1.1.3 Ultra-high strength low alloy steel - S960MC

The steel used in this study is S960MC with a yield strength of 988 MPa. S960MC is martensitic structural steel with all the characteristics of a a high strength low alloy (HSLA) steel, which creates an overlay between the two regions of (HSLA and MART) in Figure 1. Therefore this steel can be called UHSLA steel an acronym which is also used in literature [8]. S960MC is thermo-mechanically controlled processed low alloyed steel with better mechanical properties compared to conventional carbon steels and high strength steels. HSLA steels chemical composition includes alloying elements in addition to low carbon content usually between (0.05 to 0.25% C). Similarly the S960MC steel has (0.09% C) and other elements contents such as manganese, chromium, nickel, molybdenum, copper, vanadium, niobium and titanium (see section 3.1). The main strengthening mechanisms for this steel are grain refinement achieved via micro alloying and thermo-mechanical processing, solid solution strengthening (Mn, Si) and transformation strengthening (martensite). Due to the low carbon content S960MC steels have excellent formability and weldability [9].

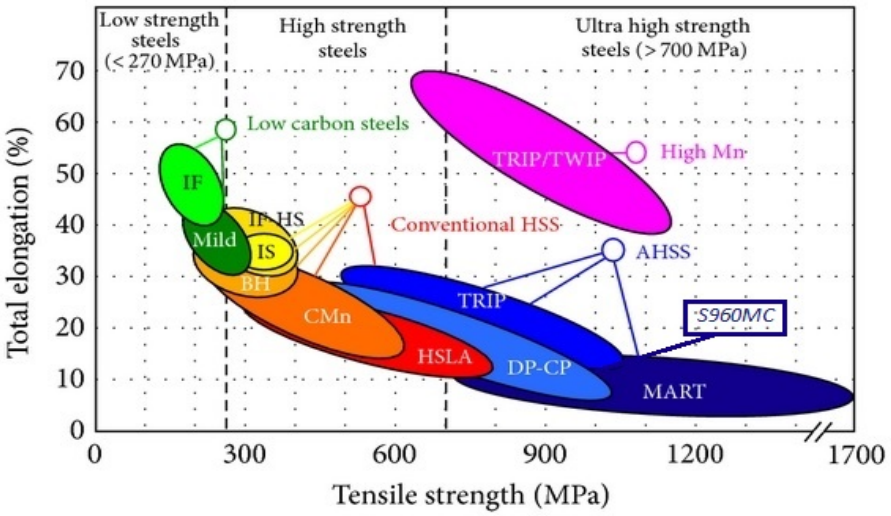

Figure 1: Steel "banana" curve, showing the tensile strength (MPa) of different steel grades in correlation to their fracture elongation (%) [2].

1.1.4 Thermo-mechanical processing

One of the main developments in the sector of ultra high strength steels especially the martensitic steels is thermo-mechanically processed UHSS. Thermo-mechanical processing is done in order to achieve optimized microstructure and mechanical properties such as high strength, excellent toughness and good weldability. Thermo-mechanical processed steel is used in high performance applications such as cranes, bridges, offshore constructions, shipbuilding and buildings [10, 11].

Historical background

Thermo-mechanical processed steels started in Europe with investigating steel metallurgical properties subjected to hot working by BISRA (British Iron and Steel Research Association) in the end of 1950's to 1960's. Furthermore, new thermo-mechanical processes were added to include direct quenching (controlled cooling after hot rolling and controlled rolling). Those studies included investigating the microstructure properties and its relation to the mechanical properties, precipitation behavior and wide variety of microalloying elements during and after the thermo-mechanical processes. The studies clarify for the researchers that strengthening mechanisms such as grain refinement can be used with microallying elements leading to the improvement of the strength, toughness and weldability of the processed steels. After the promising results in the 1960's a research project started in the United States to create high strength and tough steel plates to be used for submarines. The study resulted in achieving Ultra-fine grain steel with high mechanical properties using thermo-mechanical process technique. The industrial section started to develop the new technology in the 1970's, by the 1980's the process was installed in major steel plate mills in Europe and Japan. Later, further developments on thermo-mechanical processing are carried out which includes accelerating cooling,

direct quenching, modeling for hot rolling process and research and development on the ultra fine grain size as shown in Figure 2 [11].

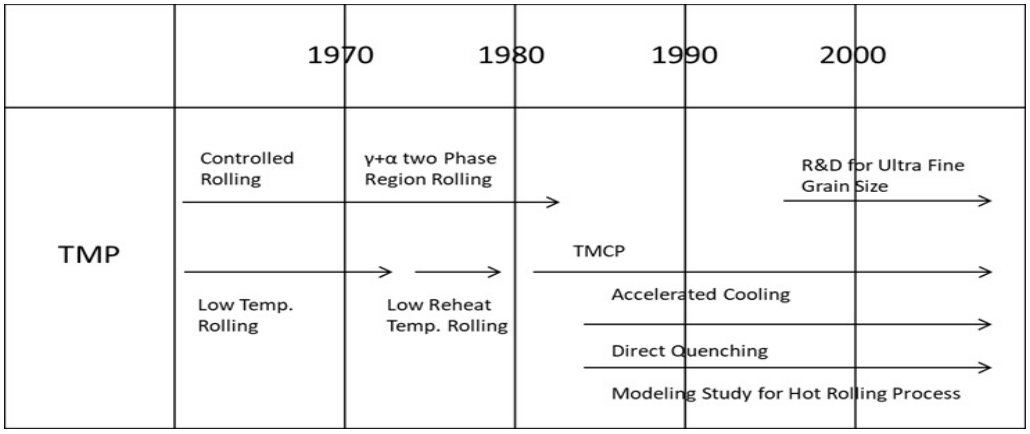

Figure 2: The time line of Thermo-mechanical processing development [11].

Thermo-mechanical controlled processing concept and process

TMCP (Thermo-mechanical controlled processed) steel strength does not only depend on the alloying and heat treatment but also on the processing technique. The high strength is achieved by direct quenching or accelerated cooling of the work-hardened austenite by the means of controlled rolling. Using the controlled rolling and controlled cooling satisfy the high strength and toughness requirements which could not be done by conventional heat treatment. TMCP is considered an effective way in terms of quality, production and cost effectiveness, compared to conventional heat treatment procedures [4, 5, 11].

Using a suitable alloy design and thermo-mechanical processes, as shown in Figure 3, is a powerful way to obtain high performance steel with optimized microstructure and excellent mechanical properties [12].

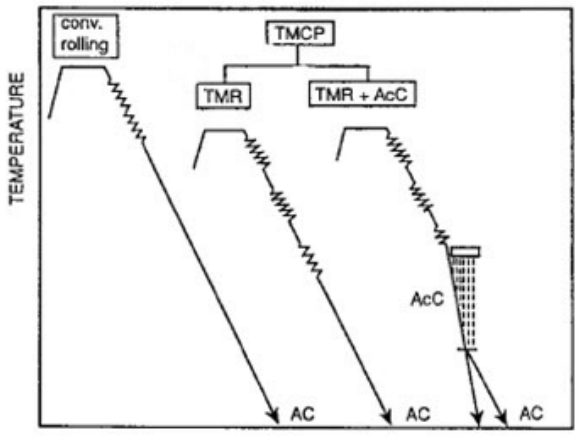

Figure 3: Conventional rolling process (left) and Thermo-mecanical controlled processes (right) [13].

Thermo-mechanical processes consist of three main stages (Figure 3). The first stage the slab reheating in which the slab is heated homogeneously in the furnace with the coarse grained microstructure. Next is the rolling stage where the plates go through three rolling methods which are done at lower temperatures compared to conventional rolling; the rolling methods used are conventional hot rolling at high forming temperatures, normalizing rolling and thermo mechanical rolling as shown in Figure 3. Finally, the cooling process at which the plates pass by AC line (Air cooled line) or AcC line (Accelerated cooling line) as shown in Figure 3 [12].

1.2 Welding of steels

Welding is considered to be one of the most common joining processes. It's always a great challenge for engineers to select the proper welding process in terms of efficiency, productivity and cost [14]. This section will highlight different welding methods of (U)HSLA steels especially focusing on the beam welding technique and the issues related to it.

1.2.1 Welding of high strength low alloy steels

HSLA steels can be welded using conventional welding processes such as arc welding processes which includes; gas metal arc welding (GMAW), submerged arc welding (SAW) and flux cored arc welding (FCAW) usually the arc welding processes are used due its cost effectiveness, flexibility and convenience [14]. Other welding techniques used includes beam welding technology such as electron beam welding (EBW) and laser beam welding (LBW) and hybrid welding technology such as laser hybrid welding (LHW).

In order to maintain the high strength and toughness, welding parameters should be carefully adjusted in order to avoid heat affected zone (HAZ) softening [5, 15] or a reduction of the toughness in the weld zone [16]. In a study by T. Mohandas et al. [15], bead-on-plate partial penetration welding of three different HSLA steels using three different welding processes, shielded metal arc welding (SMAW), gas tungsten arc welding (GTAW) and GMAW was carried out and reported that HAZ softening is usually present by different percentages depending on the HSLA steel grade, the welding technique and the parameters applied.

1.2.2 Beam welding technology

Beam welding technology refers to the processes of laser beam welding and electron beam welding. In the past decades beam welding technology has been introduced into many fields of the industry. Both processes are fully mechanized and automated which makes them more promising for future applications. Wei Guo et al. [16] welded 8 mm thick S960 UHSLA steel plates in a single weld pass, using an autogenous laser welding process. The study concluded that there was an increase in hardness and reduction of the toughness in the weld zone compared to the base material.

1.2.3 Electron beam welding

Currently many welding techniques are available in the industry, electron beam welding is considered one of the most promising welding techniques due to its ability for deep penetration welds up to 100 mm thickness. Electron beam welding technique is used in many applications and industries such as nuclear, aerospace, power generation, automotive, oil and gas industry and medical industry. Those applications need precise, narrow and defect free welds which sometimes is hard to achieve with conventional welding techniques [17, 18].

History

The development of electron beam welding technique started during the fifties. In the 1950's Karl-Heinz Steigerwald realized that small samples were melting if he increased the beam current in the transmission electron microscope. Electron beam welding was first used in 1958 to butt weld 5mm thick plates of Zircaloy by Steigerwald. During the same time in France, Dr. Jacques-Andre Stohr was conducting experiments to weld reactive materials with x-ray tube systems. The science behind the fusion welding technique started to evolve and in the early sixties high voltage electron beam systems were produced and sold by Carl Zeiss Company in cooperation with Hamilton Standard [19].

Electron beam welding concept

Electron beam welding is a fusion joining process. The process briefly consists of a focused beam of electrons generated by the cathode and accelerated towards the anode, focused by electric and magnetic lenses to perform the fusion joining process in vacuum.
Electrons are generated by thermal emission using the cathode and applying current, the free electrons need to be accelerated to have high kinetic energy to form the electron beam, which will be used for the welding process. High voltages in the range of 60 kV to 150 kV [18], are used to accelerate the electrons. After the electrons were accelerated to high speeds with sufficient kinetic energy they form the electron beam. The electron beam needs to be focused in order to deliver the power density for welding process, therefore the beam is focused and narrowed by a magnetic lenses, leading to a directed electron beam towards the work piece. When the electron beam impinge the work piece the kinetic energy transformers into thermal energy, giving sufficient energy input a vapour capillary as known as keyhole is formed and surrounded by molten material through the entire thickness. Finally the molten material solidifies forming the weld seam, see Figure 4 [18].

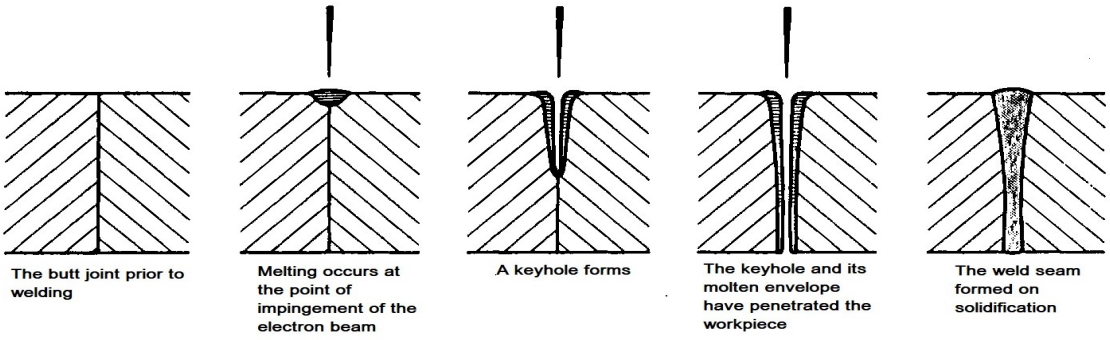

Figure 4: Stages of deep penetrating welding [18].

Electron beam welding equipment

The Electron beam welding device as shown in Figure 5 consists of three main sections, in addition to the vacuum pumps and the control unit. The first section is the beam generator in which the beam is generated. The second section is the beam forming and guidance section where the beam is formed, focused and guided to the work piece. The third section is the working chamber where the work piece is placed.

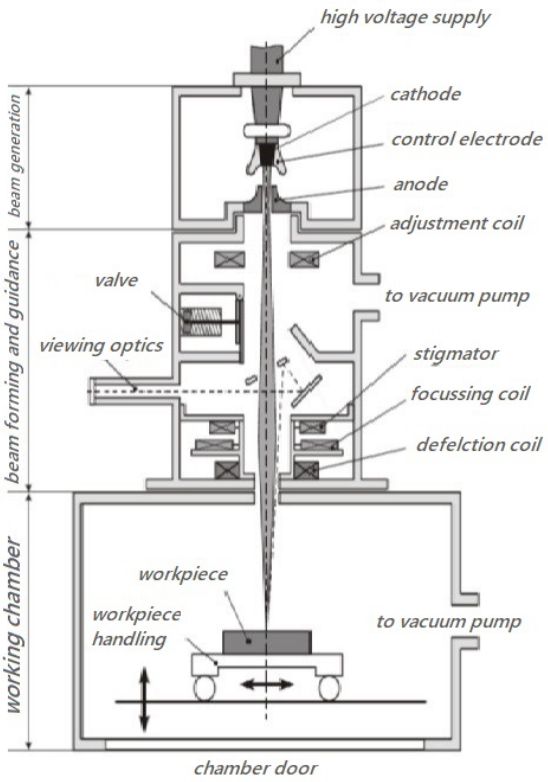

Figure 5: Schematic view of an electron beam welding machine [20].

Beam generator

The beam generator section is responsible for the beam generation via the electron gun, see Figure 6. Since electrons are charged particles, they are influenced by electric fields. A high voltage is applied between the cathode and anode. The electrons are accelerated from the source (cathode) to the positive electrode (anode) as a result of the Coulomb force acting on the electrons. Electrons absorb energy created by the potential difference which leads to acceleration, the energy absorbed by the electrons is determined by the difference of the voltage between the cathode and anode. Accordingly in electron beam welding the accelerating voltage is the main parameter to regulate the speed and thereby the energy of electrons. At a common accelerating voltage of 150 kV used for welding and in a sufficient vacuum, electrons reach two thirds the speed of light [18], see Figure 7.

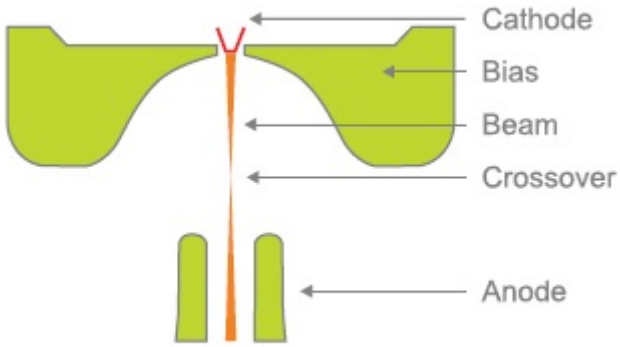

Figure 6: The electron gun, electrons are accelerated from the cathode to the anode through the bias (Wehnelt electrode) [21].

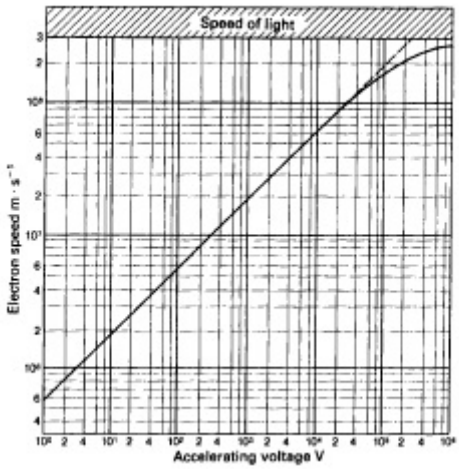

Figure 7: The relation between the accelerating voltage and the electrons speed [18].

Beam forming and guidance

After the electron beam is accelerated from the electron gun, the electron beam is narrowed and directed using magnetic lenses, see Figure 8. The magnetic lenses are used to focus the electron beam using a similar concept of optics. The magnetic lens focus the electron beam using a coil with electric current that generates a magnetic field which influences the negatively charged electrons. The magnetic lens is easily controlled by adjusting the lens current leading to a focused electron beam on the surface of the work piece.

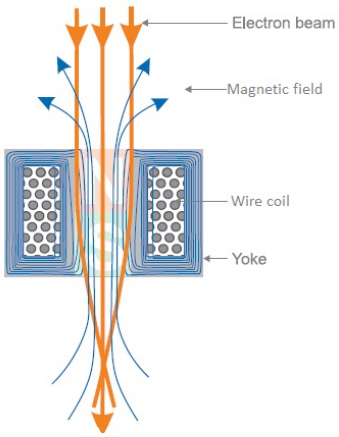

Figure 8: Magnetic lens is used to focus the electron beam by applying magnetic field [21].

Beam deflection system

The beam deflection system consists of four coils (magnetic multi-poles) perpendicular to the beam to create a magnetic field. This magnetic field allows the electron beam to be deflected into any position on the work piece. The beam deflection system is also used to oscillate the beam by adjusting the frequency and the current supplied to the coils to achieve limitless number of simple and complex shapes on the work piece such as parabola.

The beam deflection system is used to deflect the beam, see Figure 9 or to correct the beam. It is also used to correct the astigmatism as shown in Figure 10 [21].

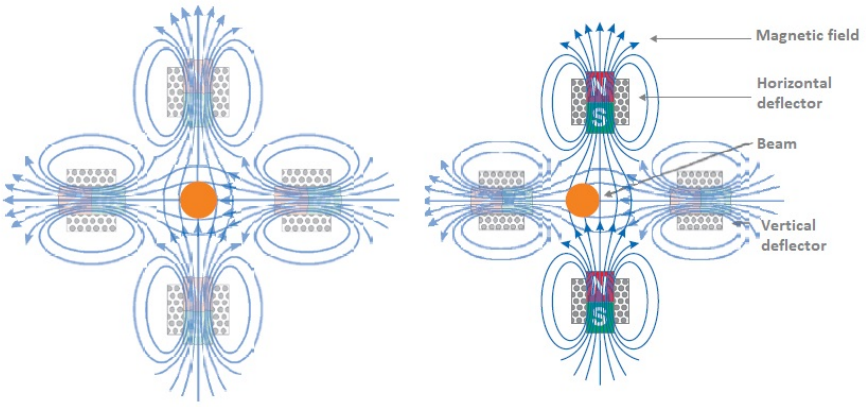

Figure 9: Centered electron beam (left), deflected Electron Beam using magnetic lens(right) [21].

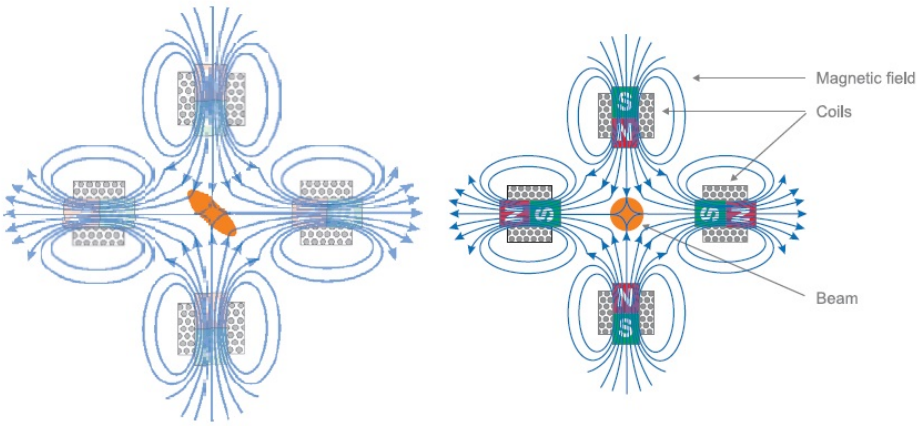

Figure 10: An electron beam with astigmatism(left),corrected astigmatism after applying magnetic field (right) [21].

Deflection systems in modern devices enable the conduction of electron beam welding with multiple beams almost at the same time (high frequency beam is deflected, which creates the "existence" of more than one beam). Multiple-beam welding is used in welding multiple joints simultaneously or in welding with pre-heating and/or post weld heat treatment processes as shown in Figure 11 [21, 22].

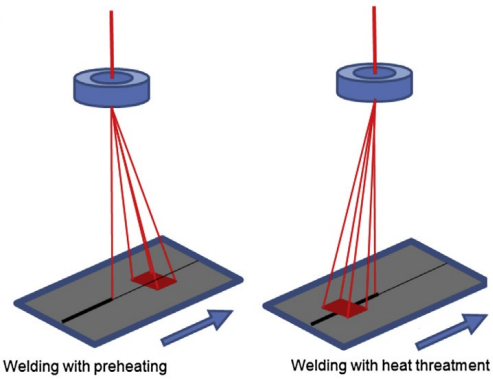

Figure 11: Schematic representation of electron beam welding with preheating (left) and post weld heat treatment (right) [22].

Working chamber

The third section of the electron beam welding machine is the working chamber, see Figure 5. The working chamber is where the welding process occurs in suitable vacuum. It is connected to the beam generator and the lenses column. The work piece is mounted at the chamber, in most of the electron beam welding devices the work piece is moving and the electron beam is fixed. In some devices the work piece is fixed and the beam can be manipulated. Depending on the machine some other options are mounted in the working chamber such as temperature measuring devices and filler metal wire.

Electron beam welding parameters

In the electron beam welding process different penetration depths and weld shapes can be achieved using different parameters in order to get the desired weld. Those parameters are adjusted in order to avoid weld defects. The welding parameters are adjusted depending on the application, material, thickness and the weld type [23]. The parameters are adjusted using the control unit of the electron beam welding equipment.

The main parameters are accelerating voltage, beam current, lens current, focal position, welding speed, beam deflection, figure and frequency. For electron beam welding process the parameters are usually implemented by the operator; depending on the weld type and the material the parameters are optimized. To get a better understanding of the main welding parameters this section shows a brief description about the key welding parameters for the electron beam welding.

- **Accelerating voltage, U** (kV)

The accelerating voltage determines the kinetic energy of the accelerated electrons and influences the power density. It is one of the main parameters due to its influence on the power density and beam diameter. Mostly, operators use accelerating voltages in the range of 60 kV to 150 kV. The accelerating voltage can be compensated by adjusting the beam current, Equation 1.1 shows that accelerating voltage, the beam current and welding speed are the main inputs for the total heat input. The energy input is mainly responsible for penetration depth. The keyhole in EBW is trapping the energy from the electron beam. Therefore, the efficiency of the electron beam is very high compared to other welding techniques, see Figure 12 [24]. It is recommended to use high accelerating voltage and low beam current in order to achieve a small beam spot at the focal point [18, 25].

$$Heat\ \ input = \eta \frac{UI}{v} = \eta \frac{P_{beam}}{v} \tag{1.1}$$

Where:

U = beam accelerating voltage, (V)

I = beam current, (A)

P = beam power, (W)

v = travel speed, ($mm\,s^{-1}$)

η = fusion efficiency, (-)

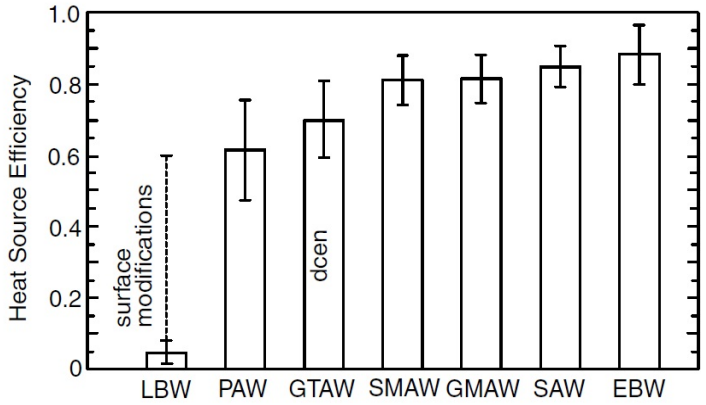

Figure 12: Heat source efficiencies in several welding processes [24].

- **Beam current, I** (mA)

  Beam current is one of the critical parameters that can be adjusted by the operator to reach a certain penetration depth. For a fixed voltage and welding speed, by increasing the beam current a higher penetration depth is achieved for thick welds. The beam current should be adjusted in order to penetrate through the work piece without sputtering or removing the material.

- **Welding speed, v** ($\mathrm{mm\,s^{-1}}$)

  It is the movement of the work piece relative to electron beam, which determines the heat input into the work piece in conjunction with the accelerating voltage and the beam current (see Equation 1.1). Adjusting the welding speed determines the heating and cooling rates, depth penetration and the fusion zone [23]. Equation 1.1 shows that welding speed is a parameter for the heat input equation by increasing the welding speed the heat input decreases which decrease the penetration depth [18].

- **Lens current and focal position** (mA)

  The electron beam is focused with an electromagnetic lens to achieve high power density and to be directed precisely on the work piece. Three different focusing positions can be achieved, normally focused, under focused and over focused on the surface of the work piece. The focal point position is adjusted via the lens current and is measured in milli amperes (mA). Depending on the welding machine, usually a fixed value (u) leads to normally focused beam on the surface of the work piece, if the value is subtracted (u-) the beam is under focused which means that the focal point is below the surface of the work piece and if the value is added (u+) the beam is over focused which means that the focal point is above the work piece, see Figure 13 [18].

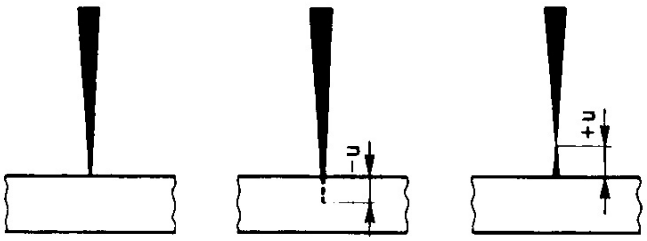

Figure 13: Different focal positions; left: normally focused, middle: under focused and right: over focused [18].

- **Beam deflection (Beam Oscillation)**

  The electron beam is deflected by applying current through the magnetic dipole deflection system. The beam deflection is related to beam oscillation.

The beam oscillation is a periodic deflection done by varying the applied current [23, 26]. The main parameters for beam oscillation are:

- The weld beam figure defines the shape of the beam from a simple circle or point to more complicated figures including images.
- Amplitude in X and Y directions in mm.
- Frequency (Hz) is the rate in which the beam cycles the figure per second.
- Orientation of the profile in relation to the welding direction.

Characteristics of electron beam welding

As the industry is dynamically developing and constantly seeking new technologies to increase the quality of welding, high quality welded joints can be achieved using Electron Beam welding (EBW) technique. The EBW technique ensures high welding speeds, narrow weld zone (WZ) and narrow HAZ compared to conventional welding techniques (see Figure 14) such as gas metal arc welding (GMAW) and plasma welding [8, 22, 27].

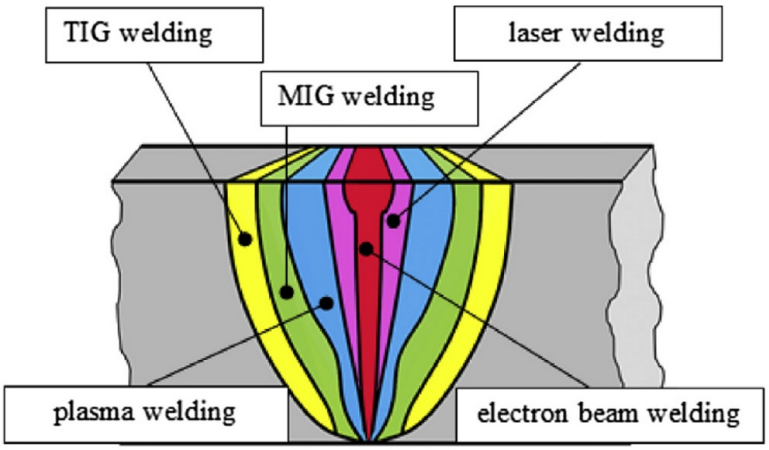

Figure 14: Geometry of butt weld of different welding processes [22].

Electron beam welding has many advantages compared to other conventional welding techniques such as:

- Electron beam welding process has a higher power density compared to conventional welding processes, which enables the keyhole effect.
- Usually it is not necessary to use filler metal which could be cost effective.
- A high purity environment because the weld is done in a vacuum chamber which minimizes contamination. Additionally no gases for protection are required.
- Electron beam welding process allows fast single pass welding of thick joints due to the keyhole effect.

- Narrow weld zone and narrow heat affected zone due to lower heat input per unit length compared to arc welding.
- The process and the parameters are all controlled using a computer system. Therefore, it is less dependent on the worker skills compared to manual arc welding techniques.

However there are some drawbacks and challenges facing the electron beam welding in vacuum [22].

- The vacuum limitation, depending on the dimensions of the vacuum chamber there is a limitation on the size of components that can be handled.
- The high cooling rates in electron beam welding can produce cracking in the HAZ and lead to porosity in the weld metal.
- Due to the narrow welding beam accurate positioning, assembling and machining of the work piece is crucial. A close tolerance is required since a gap above 0.1 mm cannot be tolerated.
- The cleaning of the parts is important. Although the vacuum is considered a high purity environment, the introduction of impurities into the system can reduce the pumping speed, efficiency of the pumping unit and the quality of the welds.
- The cost of producing electron beam welds is considered high due the high equipment cost and long production time (vacuum).

Electron beam welding of high strength steels

Interesting results were presented in studies for EBW of high strength steels. S. Bacha et al. welded 11 mm plates of high grade steel S960QL steel in a butt configuration using EBW technique and reported that the mechanical properties were satisfactory and the high strength was maintained [28].

In another study by W. Maurer et al. 6 mm plates of TMCP steel S700MC with 700 MPa yield strength were welded using electron beam welding technique and evaluated the soft zone, which occurs usually in the heat affect zone of the welded joints. It was concluded that by using characteristic electron beam welding parameters with low energy input ($E = 0.95\,kJ\,cm^{-1}$) there was an increase in the amount of the martensitic microstructure which prevented the softening [5].

Zhang et al. welded 16 mm plates of rolled and annealed 300M ultra high strength steel using EB welding technique, where post weld heat treatment was carried out and compared to the as welded condition. Results showed that the PWHT can significantly optimize the strength, ductility and impact toughness of the welded joints due to tempering [29].

1.3 Post weld heat treatment

During the welding process, high heating and cooling rates occur which lead to high temperature gradient at the weld zone. The different thermal history in relation to the weld center line changes the microstructure, such as the weld zone and the heat effected zone as well as changes mechanical properties such as higher hardness regions, residual stresses and cold cracking susceptibility. The weld properties are usually different than the base material properties which often cause problems. In many cases the weld properties determine the overall performance of the structure [30]. The different weld properties and the problems that occur during the welding process can be alleviated and/or eliminated by the means of heat treatment. Different heat treatments are employed before the welding (preheating) and/or after the welding, post weld heat treatment [30, 31].

1.3.1 Preheating

Preheating refers to the heat treatment done before the welding process. Preheating involves heating the entire base metal in a furnace, or just the region surrounding the joint by using heating torches, electrical strip heaters, or induction or radiant heaters to a specific temperature called the preheating temperature. The preheat temperature is defined by codes and standards, when no code applies there are different standards such as (European Standard EN 1011-2 Method A,B) and (AWS D1.1-2010) that provides guidelines for methods to determine the preheat temperature.
The preheat temperature is related to the carbon equivalent of steel. The carbon equivalent can be used to calculate the preheat temperature required for crack free welding. Preheat treatment is applied in order to reduce cracking and to ensure certain mechanical properties of the weld, such as toughness and hardness [32].

1.3.2 Conventional post weld heat treatment

Post weld heat treatment (PWHT) is defined as any heat treatment carried out after the welding process. Conventional post weld heat treatment is usually done in a furnace at a certain temperature for a specific time depending on the treatment. PWHT includes many different treatments which are used to improve the properties of the weldment such as hardness reduction, increasing the resistance to brittle fracture, relaxing residual stresses and material strength enhancements [31, 33, 34]. However, the influence of the PWHT process on the base material has to be considered as well. Especially for HSLA TMCP steels, due to their low carbon content and particular processing route, the thermal history of the material such as tempering resistance temperature is essential for the final mechanical properties.

PWHT is strongly dependent on the material, e.g ferrous and non ferrous metals, the microstructure and the processing. The requirement for PWHT is determined by application requirement, the service environment and Standard codes, e.g. EN 13445 for pressure vessels [35]. PWHT is usually done to enhance or eliminate undesired properties that occurred during the welding process [36] such as:

Residual stress

Residual stresses occur due to localized heating during the welding process [33]. High residual stresses in steels can increase the risk of brittle fracture by providing a driving force for crack propagation and can also lead to stress corrosion cracking depending on the material and the working environment.
The existence of high residual stresses is considered critical for chemical, oil and gas industries which operates pressure vessels. Post weld heat treatment or stress relief heat treatment reduces the stresses in the structure as result of the welding process. Heating the structure to a certain temperature defined by standards and depending on the material, then slow uniform cooling, can relax the residual stresses. [31, 33, 35].

Tempering effect

During PWHT a modification in the microstructure occurs in the weld metal, heat affected zone and for some cases in the base material, this modification is called tempering. Tempering is a process in which the martensitic structure steel is subjected to elevated temperatures in order to become more ductile.

The process involves the precipitation of carbides, the decomposition of retained austenite, segregation of carbon to lattice defects and recrystallization of the martensitic structure [37]. For martensitic steel the PWHT is important in order to temper the martensitic phase.

A study by Leijun Li concluded that PWHT changes the degree of tempering of martensite, or leads to formation of new martensite [38]. Tempering the martensitic structure leads to hardness reduction [34] and increase the toughness [31].

Effect on mechanical properties

Using appropriate post weld heat treatment conditions can lead to enhancement of the mechanical properties in the weld zone and heat affected zone, a brief description on the effect of furnace PWHT on some mechanical properties of PWHT martensitic steel joints compared to as-welded condition:

- **Hardness**
  Hardness levels are reduced after applying PWHT on martenstic steels due to tempering effect. U.Yasar et al. [34] studied the effect of PWHT at 150 °C, 300 °C and 450 °C for 2 h on the mechanical properties of high strength steel (Hardox450) welded joints. It was concluded that Hardox450 welded joints due to its carbon equivalent can be subjected to PWHT at 450 °C to decrease the hardness by 20% in the heat affected zone.

  PWHT can also lead to an increase in the hardness levels. T. Mohandas et al. [15] studied the effect of PWHT at 900 °C for 30 min on bead-on-plate partial penetration welds of HSLA steels. It was concluded that this PWHT is an effective way to eliminate the HAZ softening effect and to obtain a more uniform hardness compared to the untreated welds.

- **Toughness**
  By applying the appropriate post weld heat treatment toughness levels can be increased [31]. A.G.Olabi et al. [39] studied the effect of PWHT at 560 °C for 4 h on the mechanical properties of low carbon structural steel welded I-beam box-sections. The results showed that PWHT reduced the residual stresses and improves the toughness by 15% due to the tempering effect.

- **Ductility, fracture elongation and strength**
  An increase in ductility and fracture elongation and slight decrease in tensile and yield strengths occurs after applying PWHT. C.C Huang [40] studied the effect of PWHT on the mechanical properties of electron beam welded SAE 4120 steel plates. The PWHT was done at 530 °C for 2 h. The study concluded that the elongation of the welds increased and the strength of the welds slightly decreases after applying PWHT due to the change of microstructure from coarse lath martensite to tempered martensite.

Other applications for PWHT

PWHT can be beneficial for enhancing other properties [36] such as:

- PWHT is considered essential for creep resisting materials in order to fully develop the creep strength.
- Applying PWHT improves the diffusion of hydrogen out of weld metal.
- Carrying out PWHT procedure improves the dimensional stability during machining and the resistance to stress corrosion cracking.

1.3.3 Short cycle post weld heat treatment

Although PWHT is an important procedure for many cases in the industry to enhance the mechanical properties or to decrease undesired welding effects, some fields avoid it during maintenance and repair because it is an expensive procedure in the terms of the equipment and the duration of the process which could take several hours. Some variants such as short cycle PWHT are used which could save time and money such as temper bead technique [41] and electron beam in-situ PWHT such as; electron beam zonal heat treatment (ZHT) [42] and electron beam local post weld heat treatment [43].

Electron beam local post weld heat treatment

Electron beam local post weld heat treatment (EBLPWHT) is different than conventional furnace PWHT, since the electron beam is used to locally reheat the weld zone directly or shortly after welding, as shown in Figure 15. Electron beam local post weld heat treatment can be applied in order to alleviate toughness loss in the fusion zone due to increased hardness. EBLPWHT is considered a promising newly developed treatment that provides several advantages including saving time, energy, high precision, efficiency and higher productivity.

F.R Chen et al. [43] studied EBLPWHT on 10 mm and 20 mm thick electron beam welded joints of 30CrMnSiNi2A steel and it was concluded that the impact toughness can be improved by more than 200% at the weld zone after applying EBLPWHT, due to to structural improvement.

A similar in-situ PWHT study was done by HU Mei-juan et al. [42] to study the effect of the electron beam zonal heat treatment on electron beam welded TC4 alloy plates; the zonal heat treatment is a process that is carried out right after welding process in the vacuum chamber by employing a defocused electron beam. The result of the study shows that the ductility of the TC4 welded plates is improved due to the relief of residual stress and the microstructural changes.

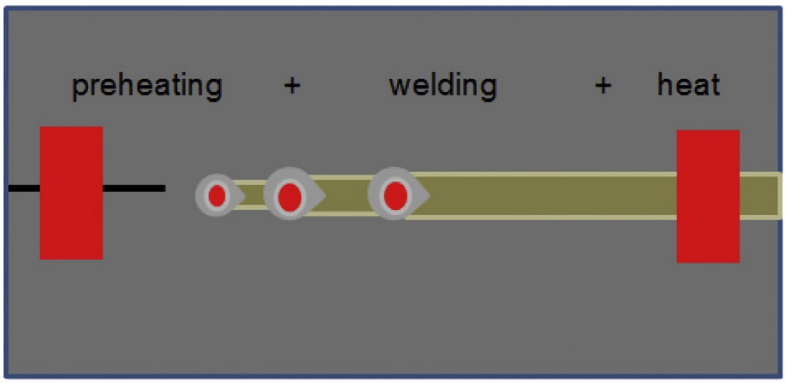

Figure 15: Schematic representation of electron beam welding with local preheating and post weld heat treatment [22].

Chapter 2

Objective

Thermomechanically processed ultra high strength steels are widely used in all fields of mechanical engineering today for weight saving purposes. Due to their low carbon content and carbon equivalent they exhibit good formability and weldability in addition to their high yield strength.

The goal of this project is to study the influence of short cycle post weld heat treatment on the microstructure and thus the mechanical properties, particularly toughness, of S960MC welds. Accordingly 8 mm sheets will be welded via electron beam welding process followed by short cycle local post weld heat treatment by EBW and alternatively physical simulation using Gleeble. The quality of the welds and the post weld heat treated welds will be assessed via materials testing and metallographic investigations.

Chapter 3

Material and Methods

3.1 Material

Sheets of structural steel S960MC with a thickness of 8 mm were used for the investigations. S960MC steel is characterized by high strength and high toughness, as shown in Table 3.1.

The chemical composition of the steel shows low carbon content to improve its weldability as well as micro-alloying elements such as Ti ,V and Nb and solid solution strengthening elements such as Mn and Si (Table 3.2). The microstructure of S960MC consists mainly of martensite and auto tempered martensite (TM) (Figure 17).

The S960MC steel is described according to EN 10027-1 and EN 10149-2 [44, 45], see Figure 16.

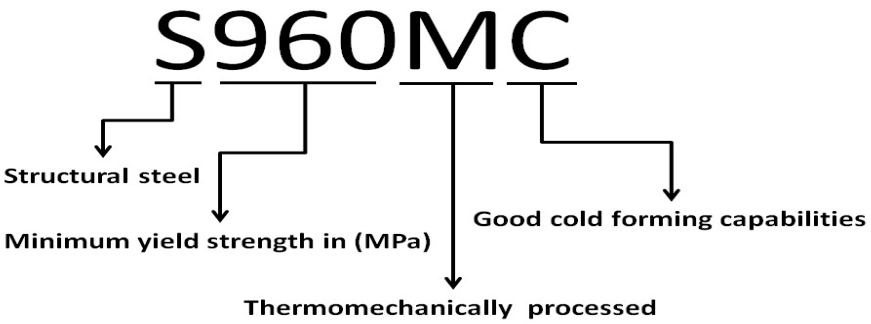

Figure 16: Description of S960MC steel.

Table 3.1: Mechanical properties of S960MC

Yield Strength (MPa)	Tensile Strength (MPa)	Fracture Elongation (%)	Impact Toughness @−20 °C J	Hardness HV10
988	1014	10.9	73.1±18	330

Table 3.2: Chemical composition of S960MC ,wt%

C	Si	Mn	Σ Cr,Ni,Mo	Cu	Σ V,Nb,Ti
0.09	0.12	1.69	1.63	0.03	0.14

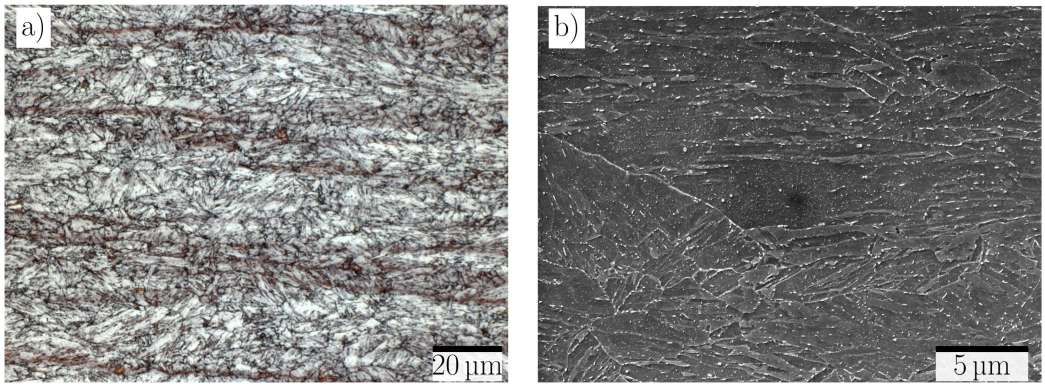

Figure 17: Microstructure of the base material, a) Light optical microscopy, LePera etched b) Scanning electron microscopy.

3.2 Methods

3.2.1 Electron beam welding

Pro beam EBG 45-150 was used for all the welds, see Figure 18, and the full specifications are listed in Table 3.3. 8 mm thick bead-on-plate and butt welds of S960MC steel were produced via EBW. For the bead-on-plate full penetration was achieved, which simulates an actual joining of the sheets.

Table 3.3: Pro beam EBG 45-150 Data

EB Gun	
Power	max. 45 kV
Accelerating voltage	max. 150 kV
Beam current	0.1 mA to 300 mA
Beam oscillation	$1\,^{\circ}\,\mu s^{-1}$
Chamber	
Volume	$1.4\,m^3$
Welding speed	$0.5\,mm\,s^{-1}$ to $100\,mm\,s^{-1}$
Vacuum	
EB Gun	$\leq 5 \times 10^{-5}$ mbar
Chamber	$\leq 5 \times 10^{-3}$ mbar

Before starting the welding process, the sheet's surfaces were cleaned with isopropanol in order to remove any contaminates. Secondly, degaussing the sheets (Figure 19) was carried out. The electron beam is quite sensitive to magnetic fields and residual magnetism in the steel, which can lead to unwanted beam deflection. During the degaussing process the steel sheets are moved multiple times through

alternating magnatic fields with decreasing amplitude in order to minimize residual magnetism below a value of $1\,\mathrm{A\,cm^{-1}}$ [18].

Figure 18: Pro beam EBG 45-150 (IMAT TU Graz).

Figure 19: Wagner magnete degaussing unit (IMAT TU Graz).

Table 3.4 lists the optimized welding parameters used for bead on plate and butt welds. A circular beam figure with amplitudes X=0.1 mm and Y=0.1 mm as shown in Figure 20 (left) was used for welding. In Figure 20 (right) the etched cross section of the as-welded sample is shown. The typical electron beam welded sheet cross section shows I-shape with a narrow weld metal, narrow heat affected zone and weld reinforcement without using filler material.

Table 3.4: Welding parameters

Parameter	Value
Accelerating voltage	150 kV
Beam focus	−31 mA
Beam modulation figure	circle
Beam oscillation	15 000 Hz
Beam oscillation amplitude	x=y=0.1 mm
Beam current	52 mA
Welding speed	27 mm s^{-1}

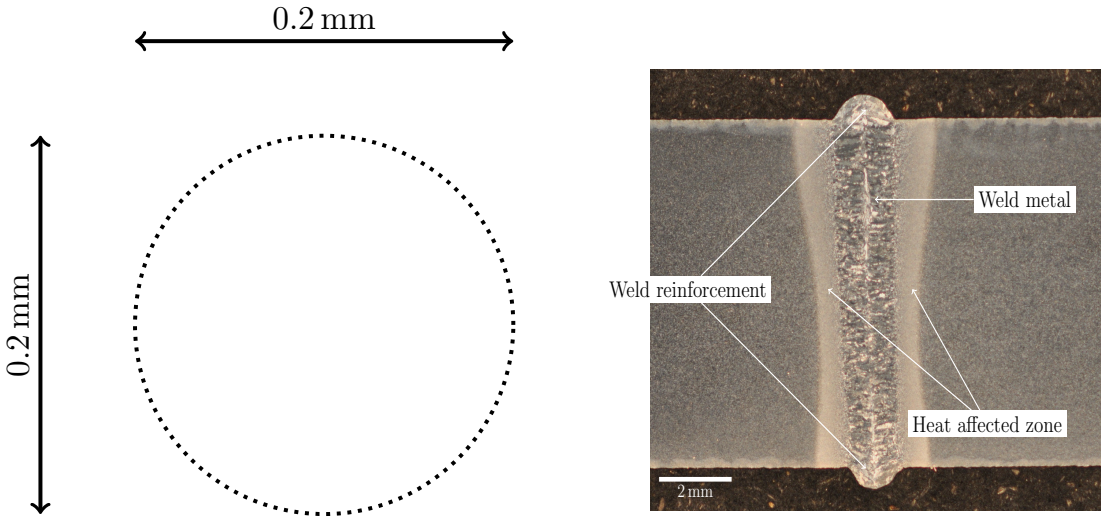

Figure 20: Circle beam figure and etched crosssection of the as-welded sample.

3.2.2 Physical simulation

Physical simulation of the PWHT was performed using Gleeble (Gleeble 3800 Basic) which operates by conductive heating with high heating and cooling rates. Physical simulation was done in order to observe the effect of the local post weld heat treatment on the mechanical properties and to test the peak temperature of the heat treatment. The welded sheet was cut into 79 mm x 7.5 mm x 10 mm (l x w x h) samples as shown in Figure 25.

The samples are subjected to uniform heating with a peak temperature of 550°C as not to exceed the annealing temperature for this steel at which BM softening occurs. Controlled cooling with $t_{8,5}$=6s, typical for GMAW. The time temperature profile was characterized using Hannerz equation [46] as follows.

$$T(t) = \sqrt{\frac{\Delta t(500 - T_o)^2(800 - T_o)^2}{300(1300 - 2T_o)t}} e^{-\left(\frac{\Delta t(500-T_o)^2(800-T_o)^2}{600e(1300-2T_o)(T_{max}-T_o)^2 t}\right)} + T_0 \tag{3.1}$$

Where,

T_{max} = peak temperature (°C)

T_o = preheat temperature (°C)

Δt = cooling time from 800 °C to 500 °C (s)

Figure 21 shows the temperature history used for the Gleeble-PWHT. The time calculated temperature profile using Equation 3.1 (PTemp), which is used as machine input and measured temperatures (TC) are perfectly aligned without any deviations.

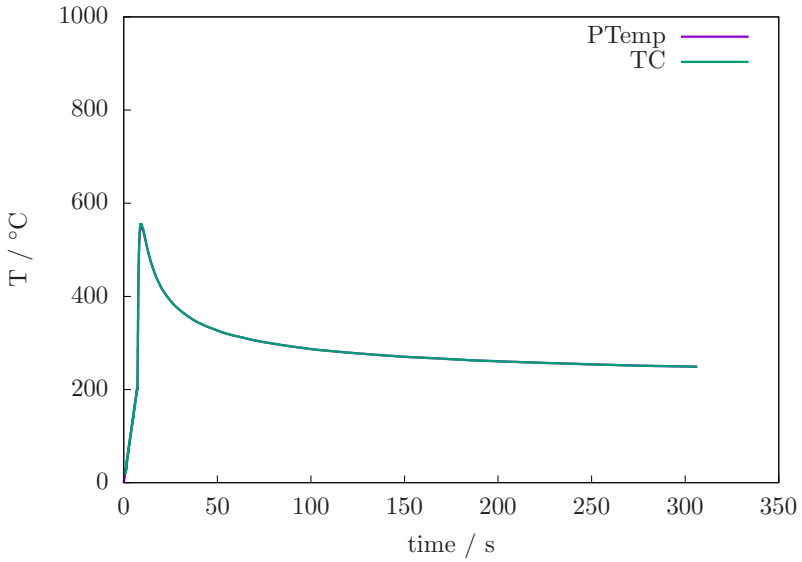

Figure 21: Gleeble temperature-time profile (PTemp: calculated temperature-time profile using Equation 3.1 for Gleeble simulation, TC: measured temperature).

3.2.3 Electron beam local post weld heat treatment

Electron beam local post weld heat treatment (EBLPWHT) is a "second welding cycle" with lower beam power which is conducted directly after the main welding.

For S960MC steel the weld zone has cooled below the martensite finish temperature at approx. 250 °C then heated to the desired peak temperature at 550 °C, which is just below the tempering resistance temperature.

Several trials were carried out using different parameters in order to achieve the desired temperature during EBLPWHT. After the several trials a suitable parameter set was obtained which is listed in Table 3.5. A concentric elliptical beam figure with amplitudes X=3 mm and Y=9 mm was used as shown in Figure 22 with a low beam speed in order to obtain more uniform heat distribution through sheet thickness at the weld area.
This EBLPWHT was applied for three different configurations on the top side, the bottom side and both sides (top side and bottom side) of the welded sheets.

Table 3.5: EBLPWHT parameters, welding direction (y-axis)

Parameter	Value
Accelerating voltage	150 kV
Beam focus	−31 mm
Beam modulation figure	concentric ellipse
Beam oscillation	15 000 Hz
Beam oscillation amplitude	x=3 mm,y=9 mm
Beam current	1.5 mA
Welding speed	1 mm s^{-1}

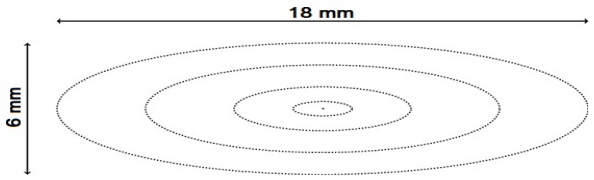

Figure 22: Beam figure concentric ellipse.

3.2.4 Temperature measurements

Temperature measurements were carried out in order to optimize the EBLPWHT parameters. K-thermocouples were used for the runs. The thermocouples were shielded with aluminum foil and ceramic shield in order to protect it from electric influence from the electron beam, as shown in Figure 23-c.

The thermocouples were mounted at different positions from the beam at the top and bottom side of the sheets, see Figure 23-a and b. The top mounted thermocouples temperature time profiles shows a step gradient at different positions as shown in Figure 23-a.

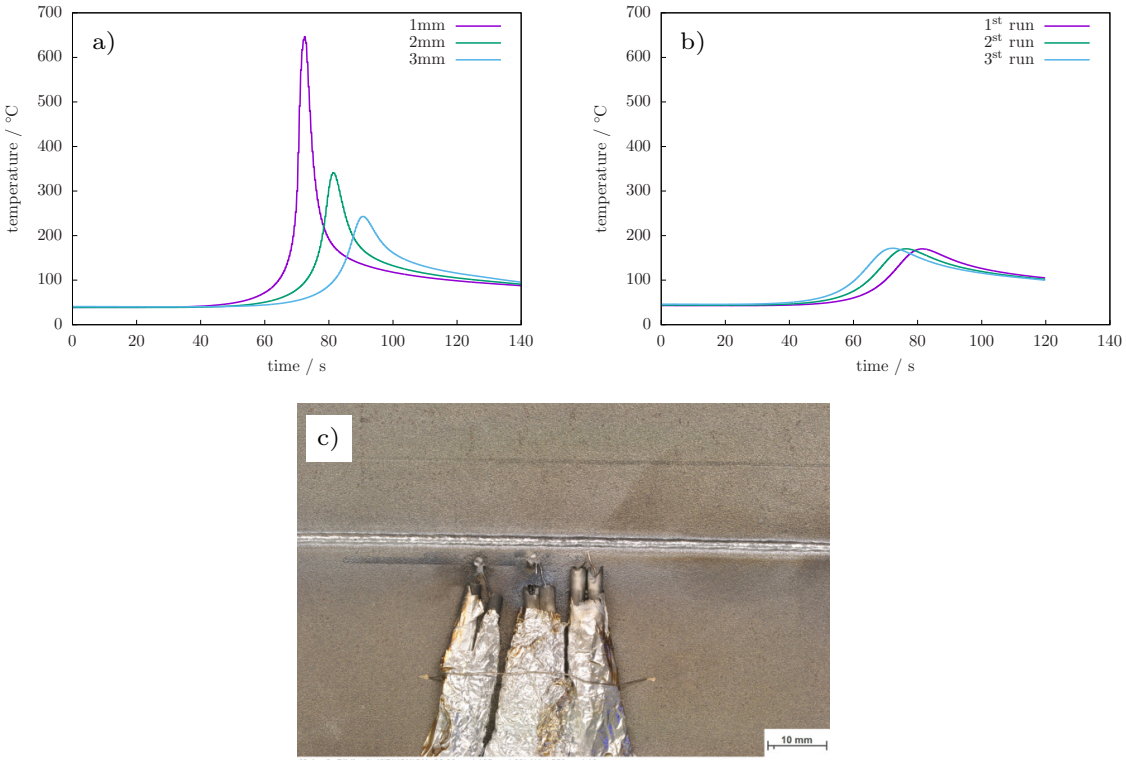

Figure 23: a) temperature profile of the topside thermocouples at different distances from the beam at 1 mm, 2 mm and 3 mm, b) temperature profile of the backside thermocouples for 3 different runs at 0 mm , c) shielded thermocouples used for the measurements.

3.2.5 Testing of welds

Hardness testing

Hardness mappings were done by means of Vickers hardness testing (Emco test M1C010) using HV0.5 standard scale. For mapping the samples, rectangular mapping was performed in order to have an overview of the hardness in the WM, HAZ and the BM throughout the sheet thickness, as shown in Figure 24. The indents are 0.2 mm apart in the X and Y direction with an indentation time of 15 s per indent.

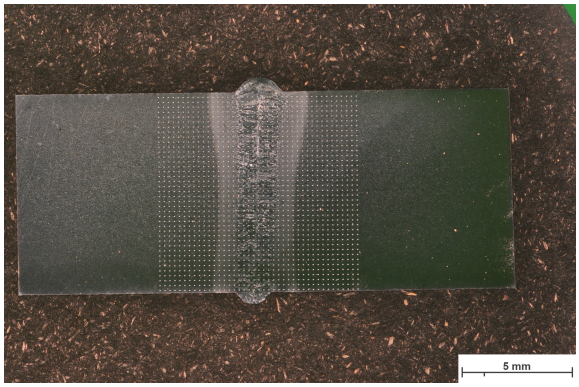

Figure 24: Hardness mapping indents.

Charpy impact testing

Sub-size charpy V-notch specimens, with dimensions of 10 mm x 7.5 mm x 55 mm were cut as shown in Figure 25 and used for impact testing (Charpy Test ISO V - 300 Joule). There is a number of investigations on the subject of correction for sub-size charpy specimens by multiplying it with a factor related to the reduced dimension [47, 48, 49, 50]. For the V-notch specimens used in our investigations the only non-standard dimension is the reduced thickness of the specimen. To compensate for the reduced thickness the recorded values were increased by the factor of 1.33 ($\frac{10}{7.5}$). The V-notch was machined perpendicular to the surface with 2 mm deep root located in the center of the weld (VWT 0/0) [51]. The samples were tested at $-20\,^{\circ}\mathrm{C}$ and $-40\,^{\circ}\mathrm{C}$.

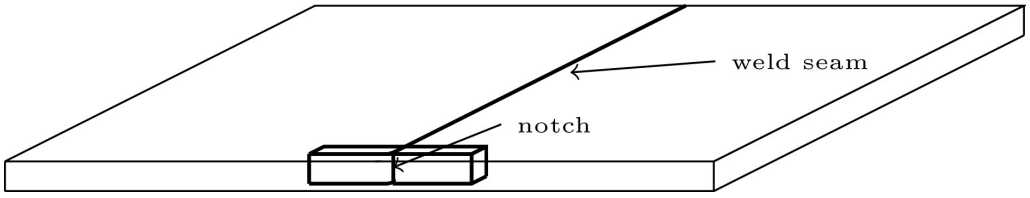

Figure 25: Position of charpy specimens in the welded sheet.

Tensile testing

Flat tensile tests were carried out across the weld according to DIN EN ISO 6892-1 and DIN 50125 [52, 53] using Universal test machine BETA 250 equipped with laser extensometer array (non-contact) for fracture elongation measurement. The samples were taken across the weld seam with the weld metal in the middle to determine the tensile strength and the yield strength of the weld, see Figure 26.

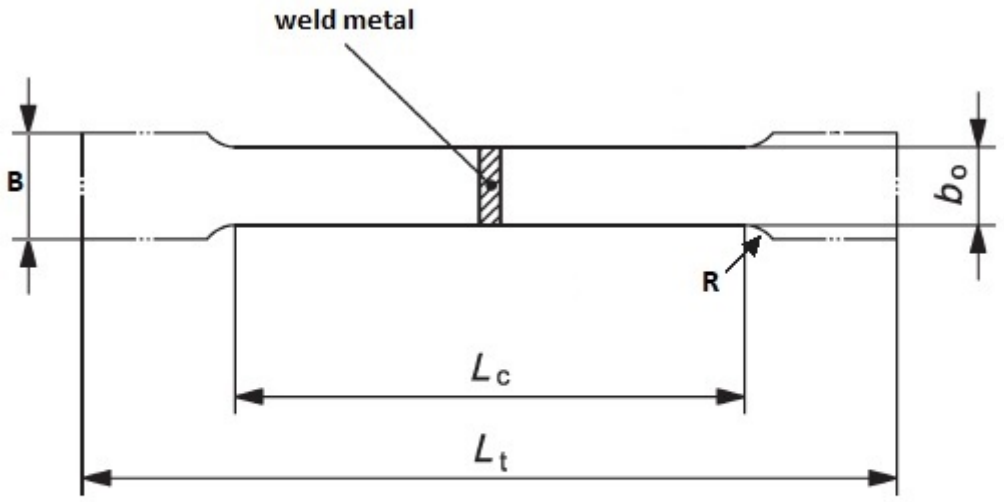

Figure 26: Tensile test specimen.

Dimensions,

- Parallel length, L_c=75 mm
- Total length of test piece, l_t=250 mm
- Grip width, B=30 mm
- Original width of the test piece, b_o=20 mm
- Radius, R=35 mm

Microstructural characterization

The welded joints were cut into cross sections and embedded using multifast resin. The specimens were grinded with rotating discs (Struers Tegramin-30) using SiC grinding papers listed in Table 3.6 at 150 RPM then polished with suspended diamond liquid (DiaDuo-2) listed in Table 3.7. The polished cross sections were etched with Nital 3%. The etching duration for the light optical microscopy and scanning electron microscopy samples was (6 s to 8 s) and (2 s to 3 s), respectively.

Table 3.6: Grinding process

stage	grit size	force (N)	time (min)
1	80	60	3:00
2	180	90	3:00
3	320	90	3:00
4	500	90	3:00
5	800	30	4:00
6	1200	30	4:00
7	2000	30	4:00
8	4000	60	5:00

Table 3.7: Polishing process

stage	grain size (µm)	force (N)	time (min)
1	3	5	4:30
2	1	5	4:00

After preparing the samples the microstructure was examined using light optical microscopy (Zeiss Axio Observer Inverted) and scanning electron microscopy (TESCAN MIRA3).

Chapter 4

Results and Discussion

In this chapter, results of the bead on plate welds and the butt welds will be presented and discussed. The samples are classified into as-welded (R), EBLPWHT top side (T), bottom side (B) and both sides (P) as described in (subsection 3.2.3) and Gleeble-PWHT (G) (Table 4.1).

Table 4.1: sample classification.

Sample	Symbol
As-welded	R
Top side EBLPWHT	T
Bottom side EBLPWHT	B
Both sides EBLPWHT	P
Gleeble-PWHT	G

Mechanical tests as well as microstructure investigations were carried out for the butt welds as shown in table Table 4.3 and for bead on plate welds Table 4.2. Since bead on plate welds were trial welds not all of the mechanical tests and heat treatments were carried out because it is time consuming and the tensile specimens have to be machined externally. The tensile test was not carried out for the butt weld G sample, because the tensile test specimens could not fit into the Gleeble jaw.

Table 4.2: Bead on plate carried out tests, were ($\surd$) shows that the test was conducted for the sample.

	R	T	B	P	G
Hardness	$\surd$	$\surd$	-	-	$\surd$
Impact	$\surd$	$\surd$	$\surd$	$\surd$	$\surd$
Tensile	-	-	-	-	-
Microstructure	$\surd$	$\surd$	-	-	$\surd$

Table 4.3: Butt weld carried out tests, were ($\surd$) shows that the test was conducted for the sample.

	R	T	B	P	G
Hardness	$\surd$	$\surd$	$\surd$	$\surd$	$\surd$
Impact	$\surd$	$\surd$	$\surd$	$\surd$	$\surd$
Tensile	$\surd$	$\surd$	$\surd$	$\surd$	-
Microstructure	$\surd$	$\surd$	$\surd$	$\surd$	$\surd$

4.1 Hardness testing

Figure 27 and Figure 28 shows hardness mappings across the bead on plate and butt weld tested samples. The color scale in the mappings is identified by the blue, green and red color ranges which represent low (approx. 250 HV 0.5), BM average (approx. 330 HV0.5) and high (approx. 450 HV0.5) hardness levels.

4.1.1 Bead on plate welds

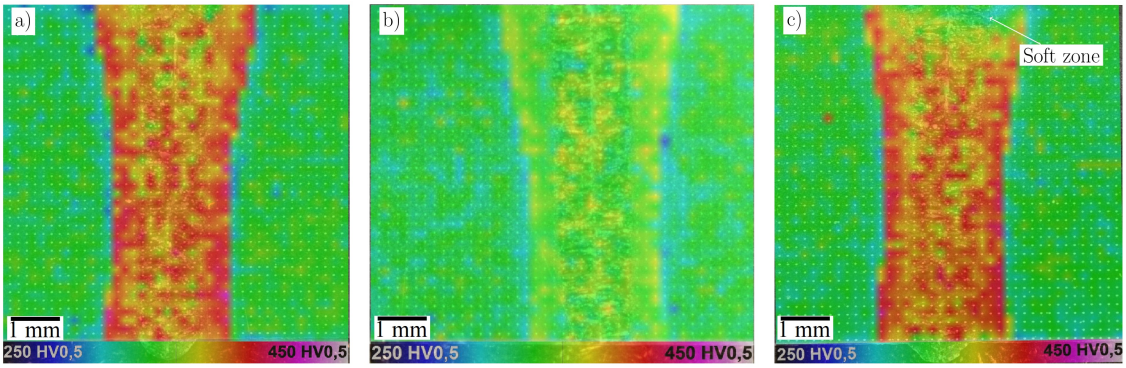

Figure 27: Hardness mappings of as-welded (a), Gleeble-PWHT (b) and EBLPWHT (T) (c).

Figure 27 shows hardness mappings across the as-welded, EBLPWHT (T) and Gleeble-PWHT joints.

In the as-welded sample Figure 27 a) the different regions of the joint are clearly distinguishable by the different colors. The unaffected base material in green (∼330 HV0.5), the average hardness of the S960MC steel, the inter critical heat affected zone (ICHAZ) in blue, with a slightly reduced hardness (300 HV0.5) due to local softening. Adjacent to the ICHAZ is the FGHAZ with the highest measured hardness, up to 410 HV0.5, due to the fine grained martensitic microstructure. The hardness drops only slightly in the CGHAZ to around 380-390 HV0.5. The average hardness in the FZ is 375 HV0.5.

In Figure 27 b) the Gleeble-PWHT mapping shows the effect of the uniform PWHT. It's clearly observed that tempering occurred during the PWHT which eliminated the high hardness regions compared to the as-welded sample. Softening in the ICHAZ with a slightly lower hardness is present, but the hardness profile for the fusion zone is generally more uniform.

In Figure 27 c) the EBLPWHT mapping shows the effect of the localized PWHT done on the top of the sample by the electron beam. This mapping is similar to as the as-welded sample except the upper part of the WM that has lower hardness compared to the rest of the WM. The softening of this part can be compared to the tempering in the Gleeble-PWHT sample, since the same hardness level was reached. But in this case the tempering occurred only in the upper part because during the fast EBLPWHT the desired peak temperature cannot be reached through the the full depth of the sheet. A significant amount of the heat of the EBLWPHT process

went also into the weld reinforcement (see Figure 20) which was eliminated from the hardness mapping.

Table 4.4 shows the average, maximum and minimum hardness values for the as-welded, Gleeble-PWHT and EBLPWHT (T) samples. The maximum hardness occurs in the fine grained heat affected zone (FGHAZ), the minimum hardness in the ICHAZ.

Table 4.4: Measured maximum and minimum hardness values across the bead on plate weld joint as well as average hardness in the weld metal of the tested samples, HV0.5.

	max. hardness (FGHAZ)	average hardness (WM)	min. hardness (ICHAZ)
As-welded	410	375 ± 21	300
Gleeble-PWHT	368	333 ± 12	300
EBLPWHT (T)	410	370 ± 18	300

4.1.2 Butt welds

Figure 28 shows the hardness mappings across the as-welded, EBLPWHT (T) , EBLPWHT (B), EBLPWHT (P) and Gleeble-PWHT joints.

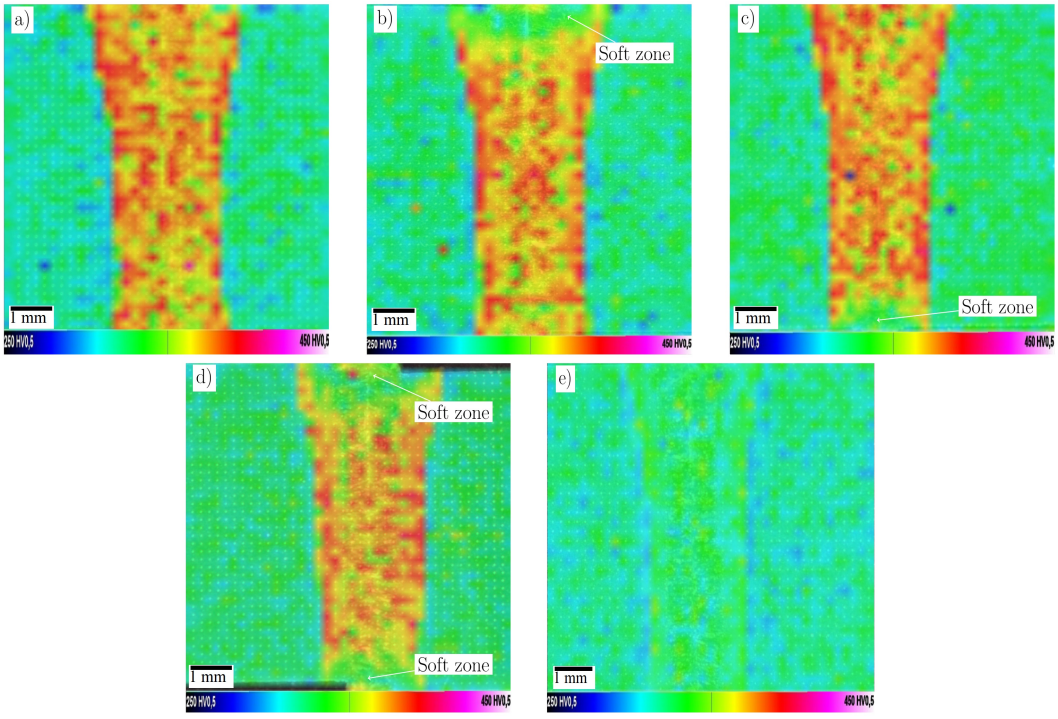

Figure 28: Hardness mappings of as-welded (a), EBLPWHT (T) (b), EBLPWHT (B) (c), EBLPWHT (P) (d) and Gleeble-PWHT (e).

The butt welds results are similar to bead on plate welds results in addition to two more configurations the EBLPWHT B and EBLPWHT P. The butt weld

hardness results will be summarized shorty in the next paragraph.

In the as-welded sample (Figure 28 a) the FGHAZ recorded the highest measured hardness due to the fine grained martensitic microstructure. ICHAZ shows slightly reduced hardness compared to the WM due to the local softening.

Figure 28 (b,c,d) shows the effect of the localized PWHT done by the electron beam on the EBLPWHT (T,B,P) respectively. The heat treated area of the WZ that has lower hardness compared to the rest of the WZ. The softening of the electron beam local post weld heat treated region is due to the tempering effect. The tempering occurred only in this region because during EBLPWHT the desired peak temperature was not reached through the full depth of the sheet. A significant amount of the heat of the EBLWPHT process went also into the weld reinforcement which was eliminated from the hardness mapping. The softened region depth at the heat treated region of the cross-section is around 1 mm.

Figure 28 e) shows the Gleeble-PWHT mapping with uniform hardness profile for the BM, HAZ and FZ, due to applying uniform PWHT across the weld zone. Tempering occurred during the PWHT which eliminated the high hardness regions compared to the as-welded sample. The softening at the ICHAZ is still present, due to local softening which is caused by the local input during welding.

Table 4.5 shows the average, maximum and minimum hardness values for the as-welded, EBLPWHT (T), EBLPWHT (B), EBLPWHT (P) and Gleeble-PWHT samples. The maximum hardness occurs in the fine grained heat affected zone (FGHAZ), the minimum hardness in the ICHAZ.

Table 4.5: Measured maximum and minimum hardness values across the butt weld joint as well as average hardness in the weld metal of the tested samples, HV0.5.

	max. hardness (FGHAZ)	average hardness (WM)	min. hardness (ICHAZ)
As-welded	403	372 ± 19	296
EBLPWHT (T)	402	368 ± 19	295
EBLPWHT (B)	405	373 ± 20	294
EBLPWHT (P)	399	360 ± 19	300
Gleeble-PWHT (G)	352	325 ± 9	298

4.1.3 Comparison between bead on plate welds and butt welds hardness values

Table 4.4 and Table 4.5 show the average and maximum hardness in the weld metal for bead on plate and butt welded samples. Both welds show similar average hardness values however the bead on plate welds show slightly higher results.

The average and maximum hardness results of the bead on plate welds and the butt welds show no influential change. The slight change of the results is in the range of the error bar. Bead on plate weld is a suitable substitution for trial butt welds due to the similarity and additionally bead on plate welds need less preparation time.

4.2 Impact testing

Impact tests were carried out on both, bead on plate and butt welds using sub-sized Charpy V-notch specimens (section 3.2.5) at $-40\,^{\circ}\mathrm{C}$ and $-20\,^{\circ}\mathrm{C}$, respectively. After the welding process the impact toughness in the weld metal of the as-welded (R) sample decreases by 60% compared to the base material (BM) at $-20\,^{\circ}\mathrm{C}$, as seen in Figure 29 and Figure 31. The PWHT samples show a slight increase in the impact toughness values except for EBLPWHT P, however due to extreme scattering of the values the reliability of those average values is questionable. The factors affecting the impact testing will be discussed in subsection 4.2.4.

4.2.1 Bead on plate welds

In Figure 29 the as-welded condition average impact toughness value decreases significantly compared to the base material. After applying EBLPWHT and Gleeble-PWHT a slight increase in the average toughness values occurred compared to the as-welded condition for EBLPWHT (T), EBLPWHT (B) and Gleeble-PWHT (G) samples. EBLPWHT (P) specimens shows lower average impact toughness value due to scattering of the values which ranges between 11 J and 39 J.

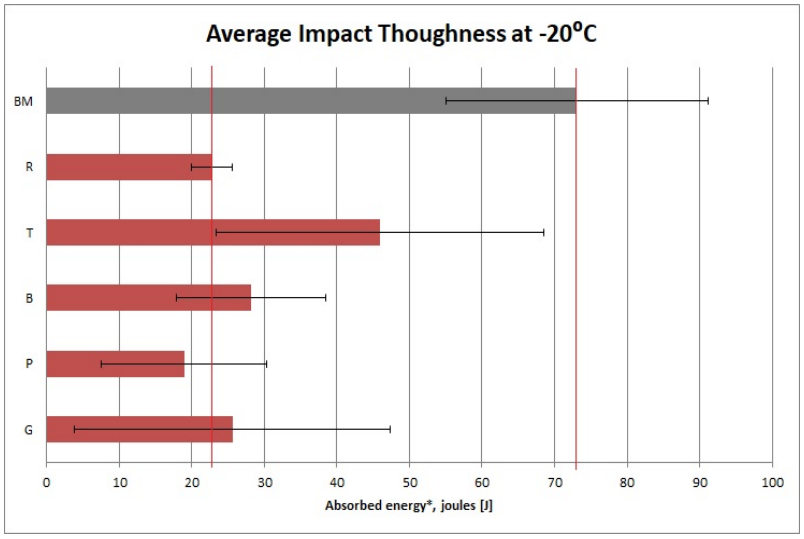

Figure 29: Average impact toughness values (J) for the bead on plate weld and the base material at −20 °C.

Figure 30 shows average impact toughness values at −40 °C. After applying EBLPWHT and Gleeble-PWHT the impact toughness values slightly increased compared to the as-welded condition [R] sample. However extreme scattering existed for T, B and G samples.

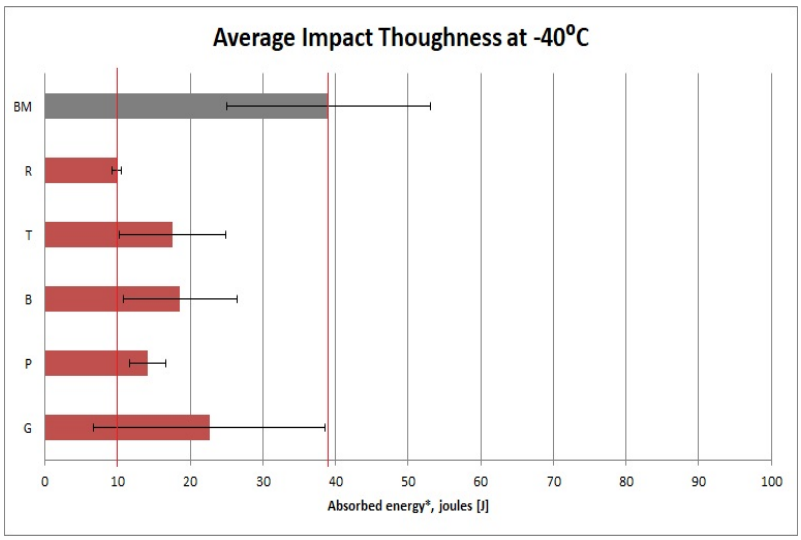

Figure 30: Average impact toughness values (J) for the bead on plate weld and the base material at −40 °C.

4.2.2 Butt welds

In Figure 31 the as-welded (R) average impact toughness value decreases compared to the base material. After applying EBLPWHT and Gleeble-PWHT a slight increase in the average impact toughness values occurred compared to the as-welded (R) for EBLPWHT (T) , EBLPWHT (B) and Gleeble-PWHT (G). EBLPWHT (P) specimens shows lower average impact toughness values. The G sample scattering values is discussed later in Figure 37, while the factors affecting the impact testing will be discussed in subsection 4.2.4

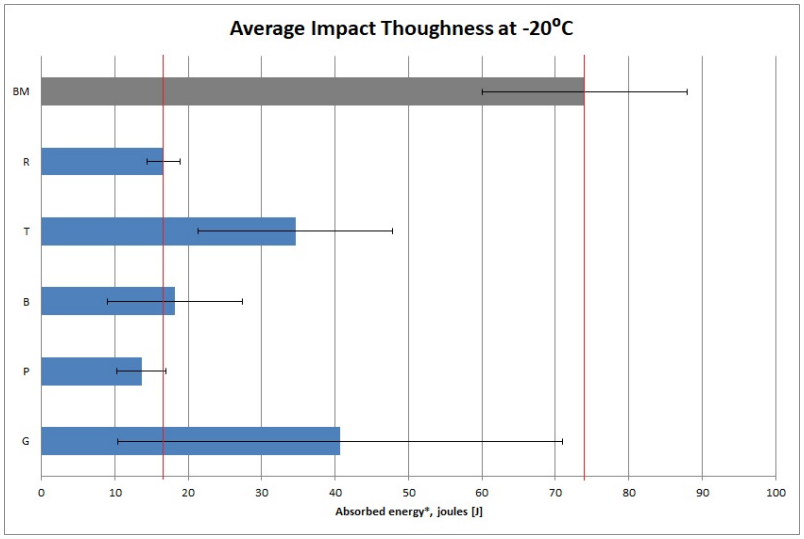

Figure 31: Average impact toughness values (J) for the butt weld and the base material at $-20\,^{\circ}\mathrm{C}$.

Figure 32 shows the average impact toughness values of the butt weld samples at $(-40\,^{\circ}\mathrm{C})$. Only for the Gleeble-PWHT sample a slight increase in the impact toughness compared to the as-welded sample, but also a high degree of scattering was observed. The other samples shows similar impact toughness values to the as-welded sample.

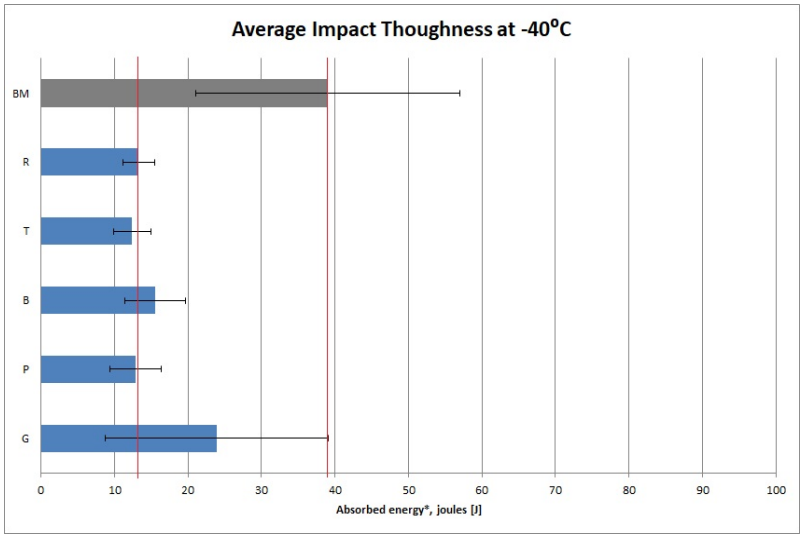

Figure 32: Average impact toughness values (J) for the butt weld and the base material at −40 °C.

4.2.3 Comparison between bead on plate welds and butt welds impact toughness values

Figure 33 and Figure 34 show a comparison between the average impact toughness values of the bead on plate and butt welds at −20 °C and −40 °C. The red bars represent the bead on plate welds while the blue bars represent the butt welds.

Figure 33 shows the average impact toughness values for the bead on plate and the butt weld samples at −20 °C. The bead on plate welds show higher average impact toughness values than the butt weld expect for the Gleeble-PWHT (G).

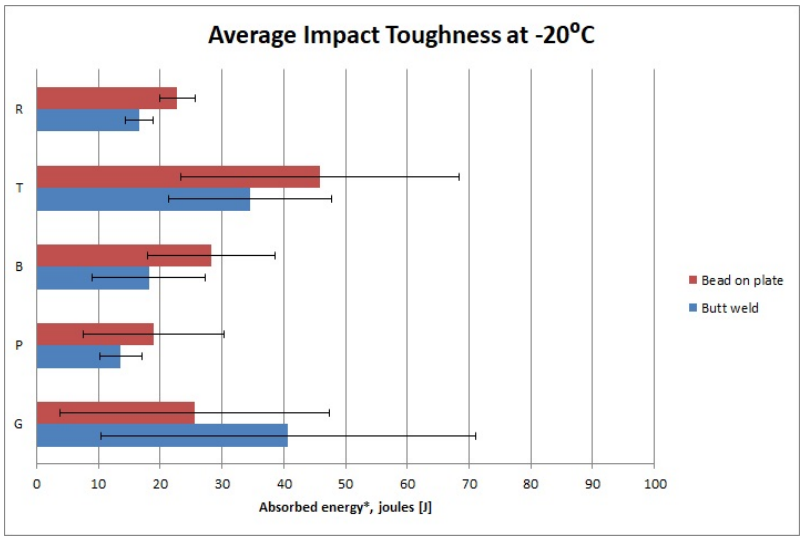

Figure 33: Average impact toughness values (J) for the bead on plate and butt welds tested samples at −20 °C.

Figure 34 shows the average impact toughness values for the bead on plate and the butt weld samples at −40 °C. The bead on plate welds again shows higher average impact toughness values than the butt weld expect for the as-welded condition (R) and Gleeble-PWHT (G).

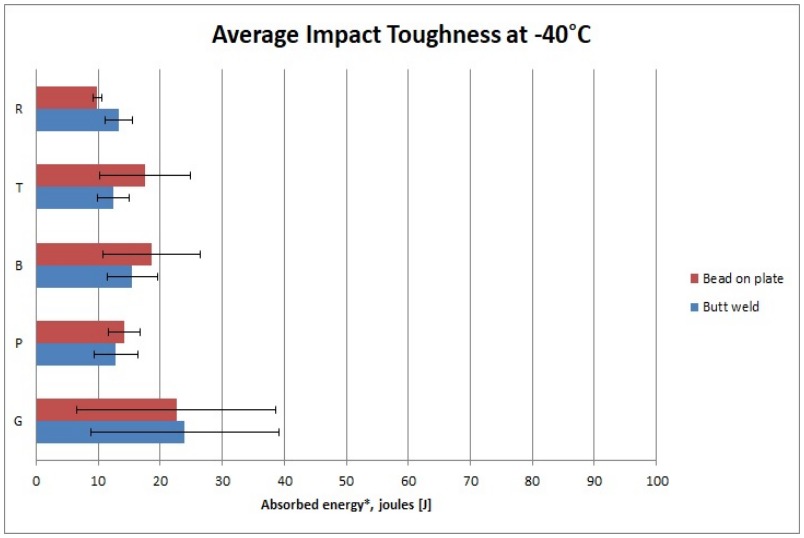

Figure 34: Average impact toughness values (J) for the bead on plate and butt welds tested samples at −40 °C.

The slightly lower impact toughness values for the butt welds may be explained by the fact that the butt welds have some additional factors affecting the welds such as the sheets misalignment due to insufficient clamping, surface roughness and any possible contamination on the the sheet edges. However most of the deviations lie well with in the error bars and therefore should not be over interpreted.

4.2.4 Factors affecting impact toughness values

Electron beam welded joints subjected to Charphy V-notch test usually suffers deviations, due to the narrow weld zone [54]. In this study an extreme scattering was observed in most of the impact toughness results. Therefore the scattering of the impact toughness values specially in Gleeble-PWHT (G) can be attributed to:

- **Positioning of thermocouples (Gleeble)**
  The positioning of the thermocouples on the samples must be taken into consideration in order to get the specific temperature of 550 °C for tempering the martensite. Figure 35 shows that a deviation of 2 mm can decrease the temperature by 65 °C. If the sample didn't reach the tempering temperature 550 °C, the tempering effect will not be completely achieved.

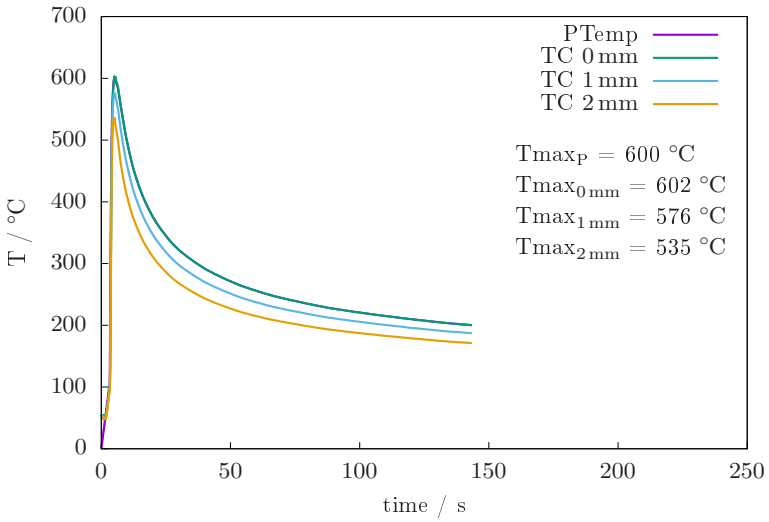

Figure 35: Time-temperature profiles and maximum temperatures during physical simulation; calculated (Equation 3.1) t-T profile as machine input (PTemp, T_{maxP}), measured t-T profiles and maximum temperatures at different positions 0 mm, 1 mm and 2 mm from peak temperature.

- **Narrow weld zone and notch location**
  The narrow weld zone of the electron beam welded joints can be problematic for selecting the notch location [54]. The V-notch should be precisely located in the weld zone of the sample, otherwise the results will be deviating. Figure 36 shows the narrow weld zone of the samples and the notch location of the samples before and after the impact test which should be precise in order to get reliable values.

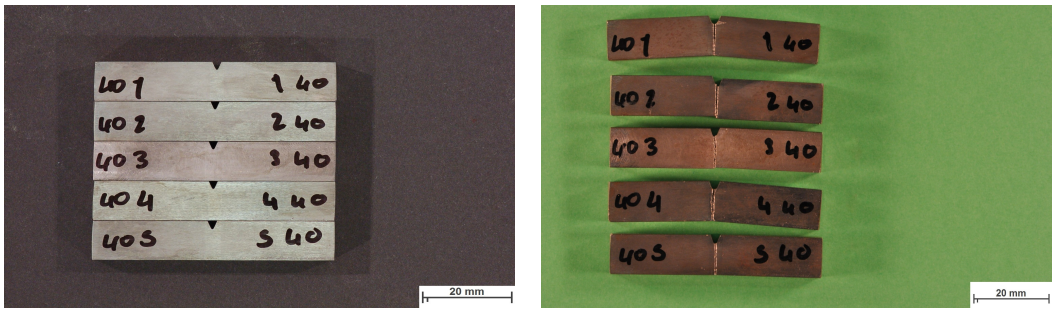

Figure 36: The notch location of Charpy V-notch samples showing the narrow weld of the EBW and the notch location, before (left) and after (right) the impact test.

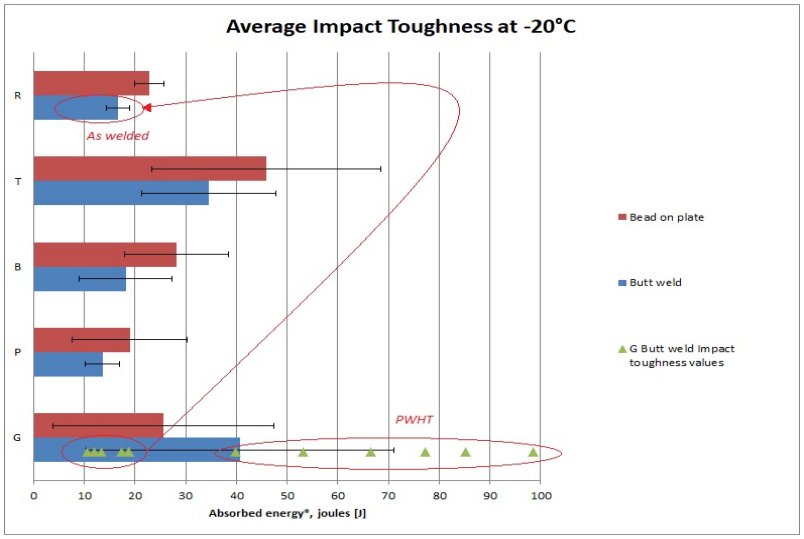

Figure 37: The scattering of the impact toughness values in Gleeble-PWHT (G) green triangles shows the individual impact toughness values of the Gleeble-PWHT (G) for the butt weld samples.

Figure 37 shows impact toughness values of the Gleeble-PWHT (G). The impact toughness values of the Gleeble-PWHT (G) can be divided into two group of values.

The first group of values are located in the range of the as welded samples as seen in (Figure 37), while the second group show higher impact toughness values. The reason that the values are scattered into two groups could be explained by the spot welding of thermocouples location in which the tempering was not fully achieved and the notch location.

- **Fracture path deviation**
  Figure 38 shows fracture path deviation sample B1, which strongly affects the impact toughness values [54]. During the impact test some samples suffered fracture path deviation, but those values were eliminated.

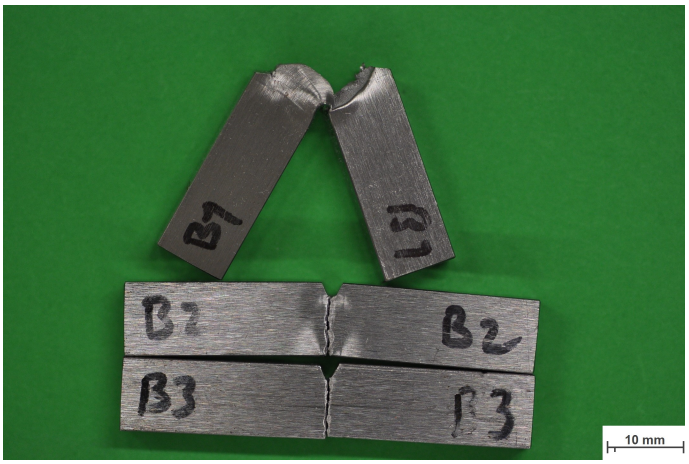

Figure 38: 3 Charpy V-notch samples after applying impact test,the first sample B1 shows fracture path deviation.

- **Asymmetric temperature profile (Gleeble)**

  Temperature profile for the Gleeble-PWHT (G) samples should be symmetric around the desired area (weld zone) to assure that uniform tempering of the martinsitic microstructure is achieved. Figure 39 shows Gleeble-PWHT (G) samples after applying PWHT, some samples show asymmetric temperature profile due to insufficient clamping. The copper jaws used in this study are not ideal for (8 mm x 10 mm) samples and can easily influence the PWHT process.

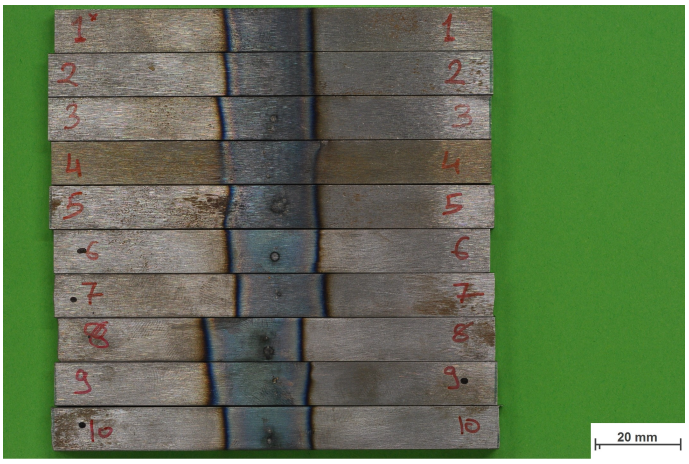

Figure 39: Gleeble-PWHT (G) samples after post weld heat treatment using gleeble.

4.3 Tensile testing

Tensile tests were done for the butt welded samples in order to make sure that the joints maintain high tensile and yield strength after applying EBLPWHT. The fracture occurred at the base material for all the samples, see Figure 41.

Figure 40 shows the stress-strain curves for the tested samples, the curves are almost identical for all samples. This shows that the steel does not loose its tensile strength after the welding and the EBLPWHT processes; the tensile strength of the base material is 1014 MPa compared to as-welded (R) 1020 MPa. After applying EBLPWHT the tensile strength slightly increase for EBLPWHT T, B and P to 1036 MPa, 1042 MPa and 1051 MPa, respectively.

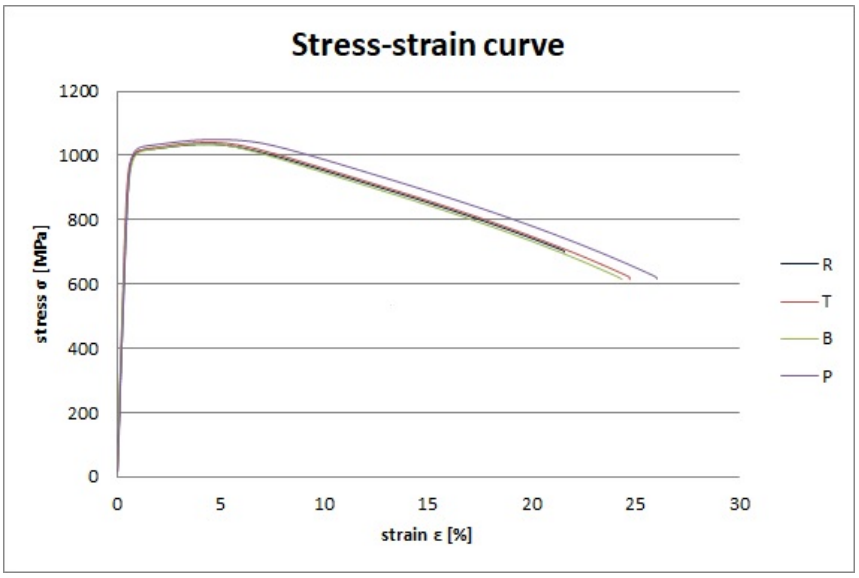

Figure 40: Measured stress-strain curve of the butt weld samples, as-welded (R), EBLPWHT (T), EBLPWHT (B) and EBLPWHT (P).

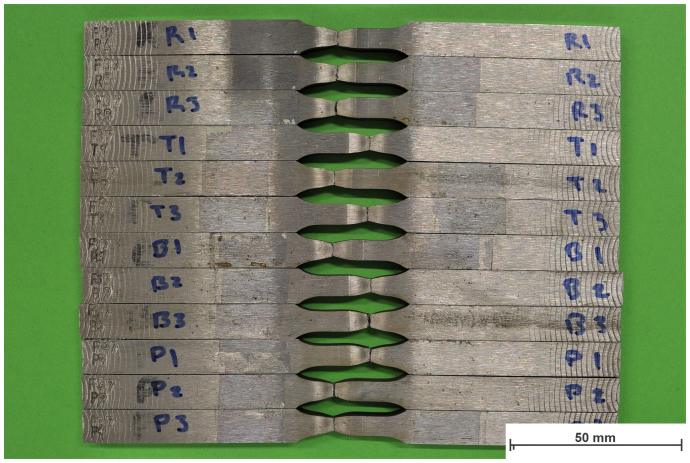

Figure 41: Butt weld tensile samples, as-welded (R), EBLPWHT (T), EBLPWHT (B) and EBLPWHT (P).

Figure 42 shows the average tensile strength values (red bars) of the butt welded samples. According to OENORM EN ISO 15614-1 [55] the average tensile strength of the welds should be the same as the base material, which is in the range of 980 MPa to 1150 MPa. The average tensile strength of the as-welded (R) is 1020 MPa, after applying EBLPWHT a slight increase in the average tensile strength occurred for EBLPWHT samples T, B and P is MPa, 1042 MPa and 1051 MPa, respectively. The average tensile strength values are listed in Table 4.6.
Figure 42 shows also the average yield strength values (blue bars) and the values are listed in Table 4.6. A slight increase of the yield strength for the as-welded (R) 993 MPa sample occurred compared to the base material yield strength 988 MPa. After applying EBLPWHT the yield strength slightly decreases compared to the as-welded (R) due to the tempering.

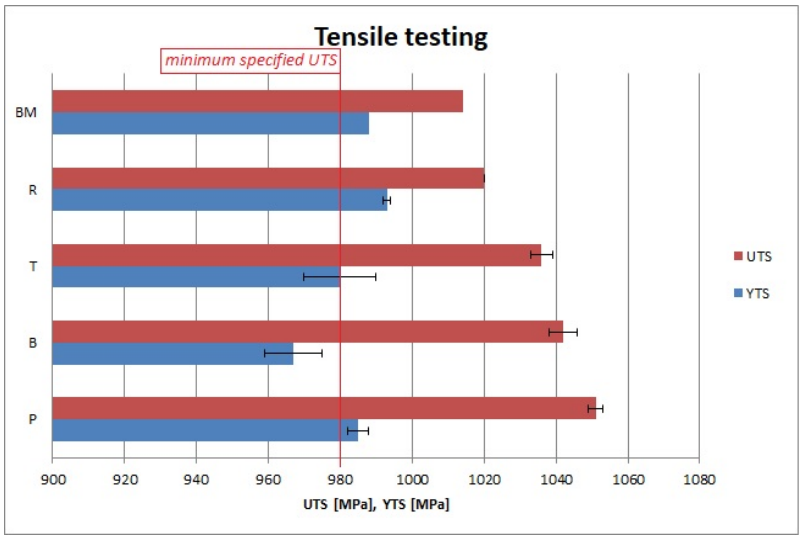

Figure 42: Measured average tensile strength (red bars) and yield strength values (blue bars) in (MPa) of the butt weld samples, as-welded (R), EBLPWHT (T), EBLPWHT (B) and EBLPWHT (P).

Figure 43 shows the average fracture elongation and the values are listed in Table 4.6. An increase of the fracture elongation for the as-welded (R) 17% sample occurred compared to the base material fracture elongation 11%. After applying EBLPWHT the fracture elongation increases compared to the as-welded (R) due to the tempering, for EBLPWHT (T) 21%, EBLPWHT (B) 22% and EBLPWHT (P) 24%.

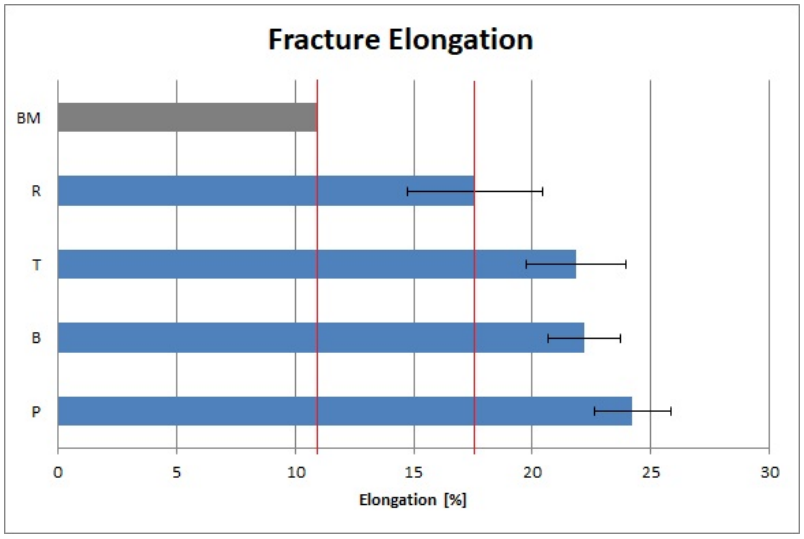

Figure 43: Measured fracture elongation (%) values of the butt weld samples, as-welded (R), EBLPWHT (T), EBLPWHT (B) and EBLPWHT (P).

Table 4.6: Measured tensile strength (UTS), yield strength (YTS) and fracture elongation average values for the butt welded samples

	UTS (MPa)	YTS (MPa)	Elongation (%)
As-welded (R)	1020 ± 0.4	993 ± 0.8	17 ± 2.8
EBLPWHT (T)	1036 ± 3.6	980 ± 10.0	21 ± 2.1
EBLPWHT (B)	1042 ± 4.1	967 ± 8.6	21 ± 1.5
EBLPWHT (P)	1051 ± 2.0	985 ± 3.4	23 ± 1.6

Short cycle PWHT has no undesirable effect on the strength properties of the welded joints. After applying EBLPWHT the yield strength was maintained on an acceptable level. A slight increase in ductile properties is detected which includes slight increase in the tensile strength and fracture elongation.

4.4 Microstructural characterization

The microstructure in the weld zone was investigated using light optical- and scanning electron microscopy. The as-welded sample was investigated and the effect of tempering in the weld metal of the PWHT samples were examined, as shown in Figure 44. The investigation was done on all the regions, but due to the significant decrease in hardness (see section 4.1), the investigation was focused on the hardness softened regions and compared to the reference. Therefore all shown images are from the region of the weld metal, where the softening in the EBLPWHT samples occurred (see Figure 27 (c) and Figure 28(b),(c),(d)).

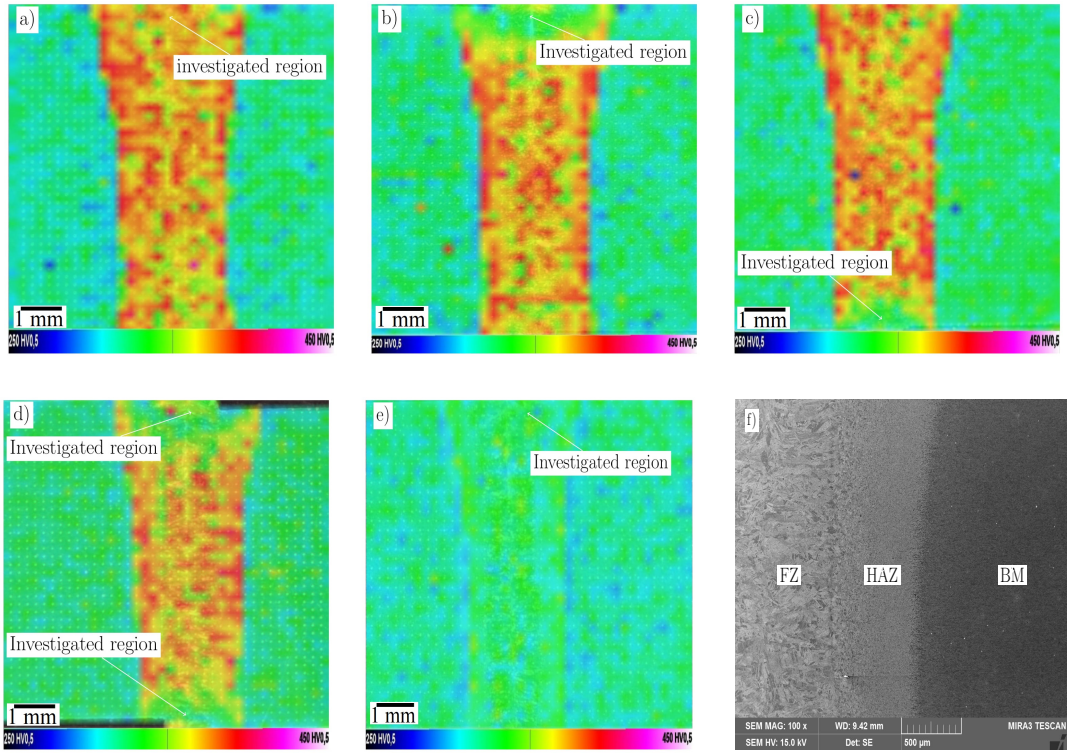

Figure 44: Investigated regions of the butt weld samples, as-welded (a), EBLPWHT (T) (b) EBLPWHT (B) (c), EBLPWHT (P) (d), Gleeble-PWHT (e) and overview of the microstructure of the as-welded condition sample showing different zones (SEM, SE) (f) .

4.4.1 Bead on plate weld

LOM

Light optical microscopy combined with Nital etching reveals the martensitic microstructure in the samples. Although some differences between the three specimens can be observed (Figure 45 a-c)), scanning electron microscopy was necessary to further characterize these differences.

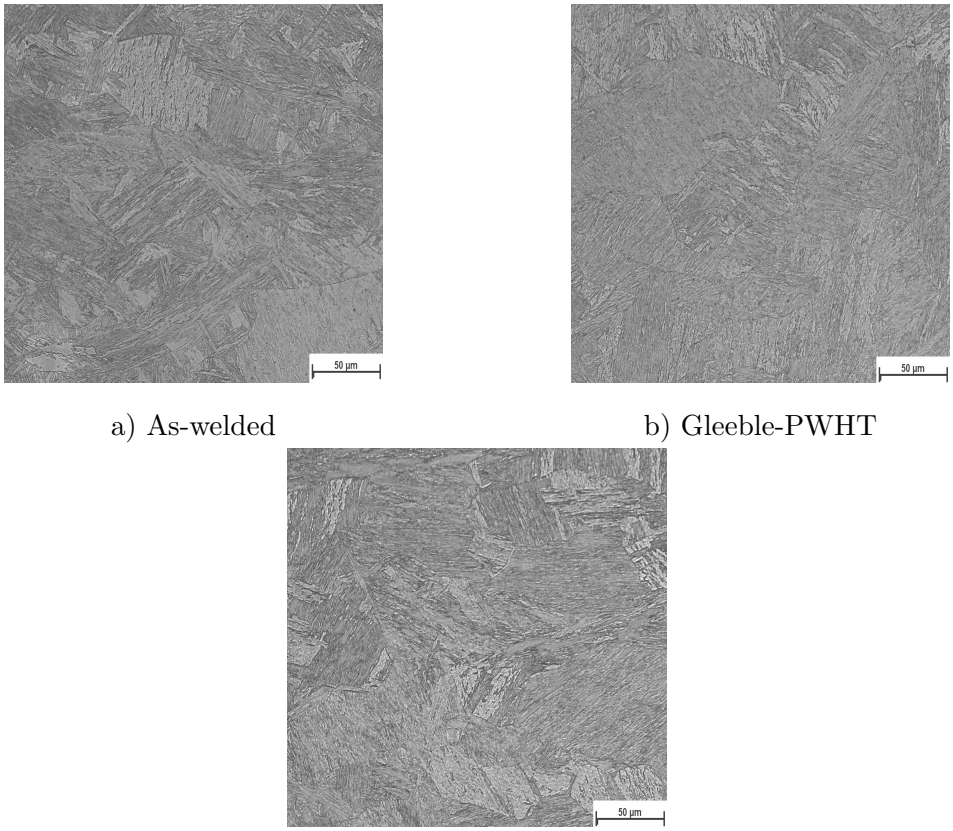

a) As-welded b) Gleeble-PWHT

c) EBLPWHT(T)

Figure 45: Microstructure of the fusion zone, Nital 3% etched, as-welded (a), Gleeble-PWHT (b) and EBLPWHT (T) (c).

SEM

Using scanning electron microscope it is possible to distinguish between lath shaped martensite structure and tempered martensite, where tempering leads to the precipitation of carbides [16, 56]. While auto-tempered martensite is formed near martensite transformation start temperature (MS) during the initial cooling after the welding process [57], tempered martensite forms after the sample has cooled below martensite finish temperature (Mf) and is reheated during PWHT. Since auto-tempered and tempered martensite can not be distinguished by SEM analysis, the designation (auto) tempered martensite will be used from now on.

Figure 46 shows representative SEM images of the three samples, as-welded (R) (top-left), Gleeble-PWHT (top-right) and EBLPWHT (T) (bottom). The pictures are from the same area as the LOM images, i.e. the top region of the weld zone. The microstructure in the as-welded sample consists of a mixture of martensite and auto-tempered martensite [16]. The microstructure in the Gleeble-PWHT and EBLPWHT (T) sample consists of a mixture of martensite and tempered martensite. The ratio of martensite structure seems to be similar between the as-welded (a) and the EBLPWHT (T) (c) sample. For the Gleeble-PWHT sample however, an increase of tempered martensite was detected.

Since tempering of martensite leads to a reduction in hardness [58, 59, 60], this increase of tempered martensite explains the significant hardness drop in the weld metal of the Gleeble-PWHT sample compared to the other two (Figure 27).

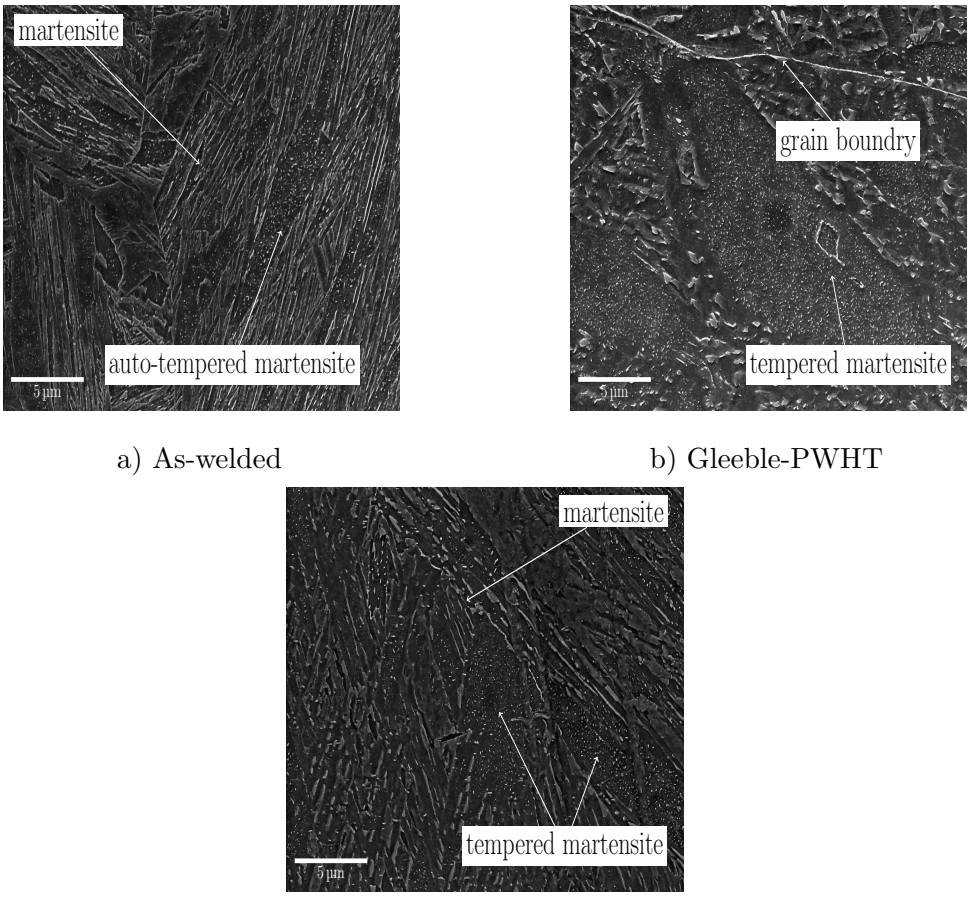

a) As-welded

b) Gleeble-PWHT

c) EBLPWHT (T)

Figure 46: Microstructure of the fusion zone, as-welded (a), Gleeble-PWHT (b) and EBLPWHT (T) (c).

4.4.2 Butt weld

SEM

Figure 47 shows representative SEM images of the butt welded samples, a) as-welded, b) EBLPWHT (T), c) EBLPWHT (B), d) EBLPWHT (P) (top region), e) EBLPWHT (P) (bottom region) and f) Gleeble-PWHT. The images were taken from the softened region, see Figure 44 and as described in the hardness section (section 4.1).

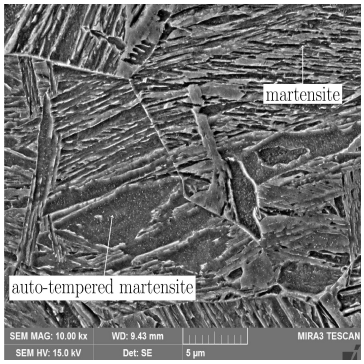

a) As-welded

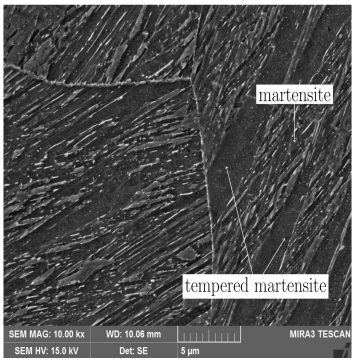

b) EBLPWHT (T)

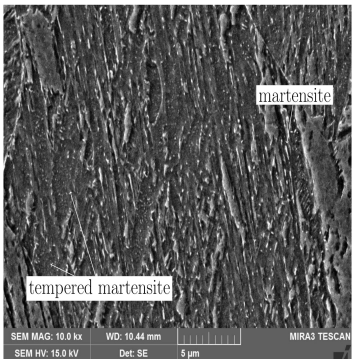

c) EBLPWHT (B)

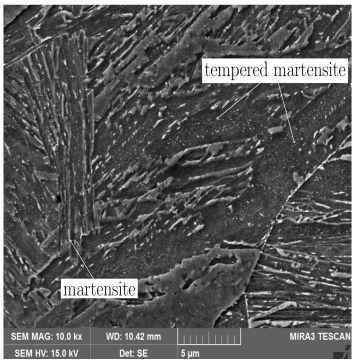

d) EBLPWHT (P) (top region)

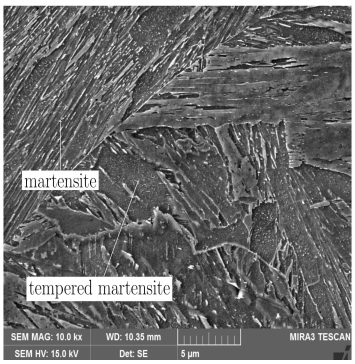

e) EBLPWHT (P) (bottom region)

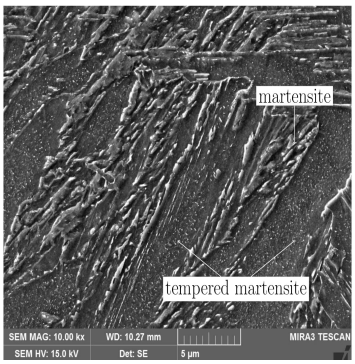

f) Gleeble-PWHT

Figure 47: Microstructure in the fusion zone, as-welded (a), EBLPWHT (T) (b), EBLPWHT (B) (c), EBLPWHT (P) (top region) (d), EBLPWHT (P) (bottom region) (e) and Gleeble-PWHT (f).

The butt welded samples show microstructure similar to the bead on plate samples and the results will be summarized shortly. The as-welded sample consists of a mixture of martensite and auto-tempered martensite. The microstructure in the EBLPWHT (T), EBLPWHT (B), EBLPWHT (P) (top region) and EBLPWHT (P) (bottom region) samples consists of a mixture of martensite and tempered martensite, while the Gleeble-PWHT sample shows an increase of tempered martensite compared to the electron beam local post weld heat treated samples.

Martensite tempering leads to an increase in the ductility and toughness properties of the material [61, 62], which could explains the increase of the fracture elongation (Figure 43), the increase of the impact toughness for the Gleeble-PWHT samples and hardness reduction for the gleeble-PWHT and locally for the EBLP-WHT treated samples.

Chapter 5

Conclusion and Outlook

5.1 Conclusion

The high energy density and localized heat input of electron beam welding enables single pass welding of 8 mm thick S960MC sheets. The obtained joints possess a narrow weld zone as well as heat affected zone. The high cooling rate of electron beam welding leads to high hardness and reduced toughness in the weld metal of the joints.

The use of physical simulation (Gleeble) to apply short cycle post weld heat treatment with medium peak temperature (550 °C), no holding time and high cooling rate leads to an increase of tempered martensite in the weld metal compared to the as-welded samples. The impact toughness in the weld metal was improved and the hardness was reduced in the weld zone, when compared to the as-welded specimens. The increase in impact toughness and hardness reduction can be linked to the higher amount of tempered martensite in the weld metal.

For the samples heat treated with electron beam local post weld heat treatment (EBLPWHT) a localized hardness reduction at the surface was found. This is caused by the steep temperature gradient in through thickness direction. Allthough no apparent increase of tempered martensite could be detected at the subjected section a slight increase in impact toughness in the weld metal was still achieved for some EBLPWHT samples.

A high degree of scattering in the Charpy V-notch results was observed which is linked to the intrinsic difficulty of testing the narrow EB joints.

The yield strength was maintained after the EBLPWHT process and even a slight increase in ductile properties was detected, which includes a slight increase in the tensile strength and fracture elongation.

Bead on plate and butt welds both showed similar results regarding mechanical properties and microstructural characteristics, before and after PWHT.

5.2 Outlook

The electron beam local post weld heat treatment shows promising results; nevertheless further investigations and studies should be conducted in order to optimize the process.

The heat input of EBLPWHT should be optimized in order to have more uniform temperature across the weld zone and to optimize the heat transfer in through thickness direction. This could be done by optimizing the EBLPWHT parameters such as the beam figure, welding speed and power.

Carrying out numerical thermal simulation for the EBLPWHT will give a better understanding regarding the temperature gradient in through thickness direction and will help to optimize the EBLPWHT parameters as well.

Conventional PWHT with 550 °C peak temperature and a longer holding time is advisable in order to compare the tempering effect of the conventional PWHT with the EBLPWHT and Gleeble-PWHT.

The influence of the different PWHT procedures on the toughness properties in the heat affected zone should be examined as well.

A systematic investigation on the physical simulation tests, regarding the positioning of the thermocouples and the asymmetric temperature profile, could help in order to avoid the uncertainty of the Gleeble-PWHT Charpy tests.

Fracture analysis of the Charpy V-notch specimens may help to explain the scattering of the toughness values. Additionally other toughness tests such as bending tests and crack tip opening displacement (CTOD), should be applied in order to eliminate the uncertainty of the Charpy tests.

Further microstructure characterization via electron backscatter diffraction (ESBD) would allow to observe the morphology changes in the martensitic microstructure due to PWHT.

Bibliography

[1] H. Bhadeshia and S. Robert Honeycombe. Iron and its Interstitial Solid Solutions. In *Steels: Microstructure and Properties*, pages 1–16. Butterworth-Heinemann, 2006.

[2] P. Suwanpinij. The Synchrotron Radiation for Steel Research. *Advances in Materials Science and Engineering*, 2016.

[3] S. Keeler, M. Kimchi, R. Kuziak, R. Kawalla, S. Waengler, H.D. Yuqing Weng, and Y. Gan. Advanced high strength steels for automotive industry. *Archives of Civil and Mechanical Engineering*, 2014.

[4] Y. NIE, C. Jia Shang, Y. You, X. Cheng Li, J. Ping Cao, and X. lai He. 960 MPa Grade High Performance Weldable Structural Steel Plate Processed by Using TMCP. *Journal of Iron and Steel Research International*, 17(2):63–66, 2010.

[5] W. Maurer, W. Ernst, R. Rauch, S. Kapl, A. Pohl, T. Krüssel, R. Vallant, and N. Enzinger. Electron beam welding of a TMCP steel with 700 MPa yield strength. *Welding in the World*, vol 56:p. 85–94, 2012.

[6] H. Spindler, M. Klein, R. Rauch, A. Pichler, and P. Stiaszny. High Strength and Ultra High Strength Hot Rolled Steel Grades – Products for Advanced Applications. *1st International Conference on Super-High Strength Steels*, 2005.

[7] World Auto Steel [Online]. Martensitic steels. `https://www.worldautosteel.org/steel-basics/steel-types/martensitic-ms-steel/`, February 2018.

[8] P. Kah, M. Pirinen, R. Suoranta, and J. Martikainen. Welding of Ultra High Strength Steels. *Advanced Materials Research*, 849:357–365, 2013.

[9] F. Brian Pickering. High Strength Low Alloy Steels. *Materials Science and Technology*, 45(4):295–301, 2006.

[10] S. Chatterjee and S. K. Ghosh. Evolution of phases and mechanical properties of thermomechanically processed ultra high strength steels. *Transactions of the Indian Institute of Metals*, 66(5-6):611–619, 2013.

[11] C. Ouchi. Development of Steel Plates by Intensive Use Of TMCP and Direct Quenching Processes. *The Iron and Steel Institute of Japan*, 41(6):542–553, 2001.

[12] S. Mandal, N. K. Tewary, S. K. Ghosh, D. Chakrabarti, and S. Chatterjee. Thermo-mechanically controlled processed ultrahigh strength steel: Microstructure, texture and mechanical properties. *Materials Science and Engineering A*, 663:126–140, 2016.

[13] Total materia Thermomechanical Control Process (TMCP): Part one [Online]. `http://www.totalmateria.com/page.aspx?ID=CheckArticle&LN=EN&site=KTS&NM=366`, February 2017.

[14] P. Kah and J. Martikainen. Current trends in welding processes and materials: Improve in effectiveness. *Reviews on Advanced Materials Science*, 30(2):189–200, 2012.

[15] T. Mohandas, G. Madhusudan Reddy, and B. Satish Kumar. Heat-affected zone softening in high-strength low-alloy steels. *Journal of Materials Processing Technology*, 88(1):284–294, 1999.

[16] W. Guo, D. Crowther, J. A. Francis, A. Thompson, Z. Liu, and L. Li. Microstructure and mechanical properties of laser welded S960 high strength steel. *Materials & Design*, 85:534–548, 2015.

[17] R. Karppi. The application of electron beam welding for the joining of dissimilar metals: an overview. *Journal of Materials Processing Technology*, 59:257–267, 1996.

[18] H. Schultz. *Electron beam welding*. Woodhead Publishing, 1993.

[19] J. Elmer, P. Hochanadel, and K. Lachenberg. *Introduction to High Energy Density Electron and Laser Beam Welding*. American Society for Metals Welding, 2009.

[20] Institute of welding and joining RWTH Acchen University [Online]. `https://internal.isf.rwth-aachen.de/index.php?id=18&L=1`, February 2017.

[21] V. Adam, U. Clauß, D. Dobeneck, T. Krüssel, and T. Löwer. *Electron Beam Welding The fundamentals of a fascinating technology*. Pro-beam AG & Co. KGaA, 2011.

[22] M. St Weglowski, S. Błacha, and A. Phillips. Electron beam welding - Techniques and trends - Review, 2016.

[23] J. Huang. *The characterization and modelling of porosity formation in electron beam welded titanium alloys*. PhD thesis, The University of Birmingham, 2011.

[24] S. Kou. *Welding Metallurgy Second Edition*, volume 822. Wiley Interscience, 2003.

[25] Aalto University-School of engineering [Online]. Electron Beam Welding. `https://mycourses.aalto.fi/pluginfile.php/142852/mod_resource/content/1/ElectronBeamWelding_en_full.pdf`, February 2017.

[26] C. Wiednig. Electron Beam Welding Alloy 625. Master's thesis, Graz University of technology, 2013.

[27] A. Rajasekhar. Effect of welding process and post weld heat treatments on microstructure and mechanical properties of AISI 431 maetensitic stainless steel. *Journal of Technical Research and Applications*, 3(3):280–285, 2015.

[28] S. Błacha, M.S. Węglowski, S. Dymek, and M. Kopyściański. Microstructural and Mechanical Characterization of Electron Beam Welded Joints of High Strength S960QL and Weldox 1300 Steel Grades. *Archives of Metallurgy and Materials*, 62(2):627–634, 2017.

[29] G. Zhang, X. Yang, X. He, J. Li, and H. Hu. Enhancement of mechanical properties and failure mechanism of electron beam welded 300M ultrahigh strength steel joints. *Materials and Design*, 45:56–66, 2013.

[30] T. Kasuya, M. Okumura, and N. Yurioka. Methods for predicting maximum hardness of heat-affected zone and selecting necessary preheat temperature for steel welding. *Nippon Steel Technical Report*, (65):7–14, 1995.

[31] B. K. Srivastava and J. Prakash. a Review on Effect of Preheating and/or Post Weld Heat Treatmemt (PWHT) on Mechanical Behaviour of Ferrous Metals. *International Journal of Engineering Science and Technology*, 2(4):625–631, 2010.

[32] H. Cable and R. S. Funderburk. Technology Transfer -The Basics. *Welding Innovation*, XIV(2):16–17, 1997.

[33] K. A. Venkata, S. Kumar, H. C. Dey, D. J. Smith, P. J. Bouchard, and C. E. Truman. Study on the effect of post weld heat treatment parameters on the relaxation of welding residual stresses in electron beam welded P91 steel plates. *Procedia Engineering*, 86(Grade 91):223–233, 2014.

[34] U. Y. Uzunali and H. Cuvalci. The Effects of Post Weld Heat Treatment on the Mechanical Properties of Tempered Martensite and High Strength Steel Welded Joints. *Advances in Structural Engineering and Mechanics*, 2015.

[35] W. J. Hall. Advanced Arc Welding Design and Practice Worldwide. *Welding Innovation*, pages 17 –18, 1998.

[36] Welding Technology Institute of Australia (WTIA). Guidance note 6: post weld heat treatment of welded structures. (6):1–10, 2003.

[37] G. R. Speich and W. C. Leslie. Tempering of steel. *Metallurgical Transactions*, 3(5):1043–1054, may 1972.

[38] L. Li, R. Wright, and S. Lesica. Effect of Post-Weld Heat Treatment on Creep Rupture Properties of Grade 91 Steel Heavy Section Welds. *U.S. Department of Energy*, (09), 2012.

[39] A.G. Olabi and M.S.J. Hashmi. The effect of post-weld heat-treatment on mechanical-properties and residual-stresses mapping in welded structural steel. *Journal of Materials Processing Technology*, 55(2):117–122, nov 1995.

[40] C. C. Huang, Y. C. Pan, and T. Chuang. Effects of post-weld heat treatments on the residual stress and mechanical properties of electron beam welded SAE 4130 steel plates. *Journal of Materials Engineering and Performance*, 6:61–68, 1997.

[41] A. S. Aloraier, R. N. Ibrahim, and J. Ghojel. Eliminating post-weld heat treatment in repair welding by temper bead technique: Role bead sequence in metallurgical changes. *Journal of Materials Processing Technology*, 153-154(1-3):392–400, 2004.

[42] M. HU and J. LIU. Effects of zonal heat treatment on residual stresses and mechanical properties of electron beam welded TC4 alloy plates. *Transactions of Nonferrous Metals Society of China (English Edition)*, 19(2):324–329, 2009.

[43] F. R. Chen, L. X. Huo, Y. F. Zhang, L. Zhang, F. J. Liu, and G. Chen. Effects of electron beam local post-weld heat-treatment on the microstructure and properties of 30CrMnSiNi2A steel welded joints. *Journal of Materials Processing Technology*, 129(1-3):412–417, 2002.

[44] European Committee for Standardization (CEN). EN 10027-1 Designation systems for steels - Part 1: Steel names. *European Standards*, 3:1–25, 2005.

[45] European Committee for Standardization (CEN). EN 10149-2 Steels for cold forming. 2013.

[46] N. E. Hannerz. Effect of Cb on HAZ Ductility in Constructional HT Steels. *Welding Journal*, page 81, 1975.

[47] W. Kim. Upper shelf energy normalisation for sub-sized charpy-v specimens. *International Journal of Pressure Vessels and Piping*, 78(7):463 – 470, 2001.

[48] Y.J. Chao, J.D. Ward, and R.G. Sands. Charpy impact energy, fracture toughness and ductile–brittle transition temperature of dual-phase 590 steel. *Materials and Design*, 28(2):551 – 557, 2007.

[49] L. E. Schubert, A. Kumar, S. T. Rosinki, and M. L. Hamilton. Effect of specimen size on the impact properties of neutron irradiated a533b steel. *Journal of Nuclear Materials*, 225:231–237, 08 1995.

[50] B. S. Louden, A. S. Kumar, F. A. Garner, M. L. Hamilton, and W.L. Hu. The influence of specimen size on charpy impact testing of unirradiated ht-9. *Journal of Nuclear Materials*, 155(Part 2):662 – 667, 1988.

[51] International Organization for Standardization (ISO). EN ISO 9016:2012 - Destructive tests on welds in metallic materials-Impact tests- Test specimen location, notch orientation and examination. 2012.

[52] International Organization for Standardization (ISO). EN ISO 6892-1:2016-BSI Standards Publication Metallic materials — Tensile testing Part 1 : Method of test at room temperature. 2016.

[53] Deutsches Institut für Normung E.V. (DIN). DIN 50125 EN Tensile Testing of Metallic Materials- Tensile Test Pieces. 2009.

[54] C. Wiednig and N. Enzinger. Toughness evaluation of EB welds. *Welding in the World*, 61(3):463–471, 2017.

[55] International Organization for Standardization (ISO). EN ISO 15614-1 Specification and qualification of welding procedures for metallic materials - Welding procedure test. 2012.

[56] W. Guo, S. Li, L.and Dong, D. Crowther, and A. Thompson. Comparison of microstructure and mechanical properties of ultra-narrow gap laser and gas-metal-arc welded S960 high strength steel. *Optics and Lasers in Engineering*, 91(April):1–15, 2017.

[57] H. Matsuda, R. Mizuno, Y. Funakawa, K. Seto, S. Matsuoka, and Y. Tanaka. Effects of auto-tempering behaviour of martensite on mechanical properties of ultra high strength steel sheets. *Journal of Alloys and Compounds*, 577(Suppl. 1), 2013.

[58] H.S. Rawdon and S. Epstein. Structure of martensitic carbon steels and the changes in microstructure which occur upon tempering. *Journal of the Franklin Institute*, 195(2):241–243, 1923.

[59] R. A. Grange, C. R. Hribal, and L. F. Porter. Hardness of tempered martensite in carbon and low-alloy steels. *Metallurgical Transactions A*, 8(11):1775–1785, 1977.

[60] S. Kang and S. Lee. Prediction of Tempered Martensite Hardness Incorporating the Composition-Dependent Tempering Parameter in Low Alloy Steels. *Materials Transactions*, 55(7):1069–1072, 2014.

[61] G. Krauss. Tempering of Lath Martensite in Low and Medium Carbon Steels: Assessment and Challenges. *Steel Research International*, 88(10):1–18, 2017.

[62] F. Zia-Ebrahimi and G. Krauss. Mechanisms of tempered martensite embrittlement in medium-carbon steels. *Acta Metallurgica*, 32(10):1767–1778, 1984.

List of Figures

Appendix

A1 Charpy V-notch test

Table A1: Measured toughness values (J) for the bead on plate weld samples as well as average toughness of the tested samples,values at $-20\,^{\circ}\mathrm{C}$

	Impact toughness[J]	Average impact toughness[J]
As-welded (R)	25, 20	22 ± 2
EBLPWHT (T)	66, 66, 63, 47, 17, 13	45 ± 22
EBLPWHT (B)	23, 23, 39, 13, 39	28 ± 10
EBLPWHT (P)	10, 13, 38, 13	18 ± 11
Gleeble-PWHT (G)	19, 11, 62, 7	25 ± 21

Table A2: Measured toughness values (J) for the bead on plate weld samples as well as average toughness of the tested samples,values at $-40\,^{\circ}\mathrm{C}$

	Impact toughness[J]	Average impact toughness[J]
As-welded (R)	9, 9, 11	10 ± 1
EBLPWHT (T)	29, 10, 14, 23, 11	17 ± 7
EBLPWHT (B)	11, 16, 29	19 ± 7
EBLPWHT (P)	11, 16, 16	14 ± 2
Gleeble-PWHT (G)	12, 11, 45	23 ± 16

Table A3: Measured toughness values (J) for the butt weld samples as well as average toughness of the tested samples,values at −20 °C

	Impact toughness[J]	Average impact toughness[J]
As-welded (R)	19, 16, 19, 13	17 ± 2
EBLPWHT (T)	53, 27, 24	34 ± 13
EBLPWHT (B)	37, 11, 13, 12, 21, 15	18 ± 9
EBLPWHT (P)	11, 11, 13, 13, 16, 11, 13, 21	14 ± 3
Gleeble-PWHT (G)	66, 11, 98, 18, 19, 53, 13, 85, 40, 77, 17, 12, 19	40 ± 30

Table A4: Measured toughness values (J) for the butt weld samples as well as average toughness of the tested samples,values at −40 °C

	Impact toughness[J]	Average impact toughness[J]
As-welded (R)	13, 11, 16	13 ± 2
EBLPWHT (T)	16, 11, 11	12 ± 2
EBLPWHT (B)	12, 21, 13	15 ± 4
EBLPWHT (P)	16, 15, 8	13 ± 3
Gleeble-PWHT (G)	11, 16, 45	24 ± 15

Figure A1: Butt weld as welded Charpy V-notch samples after applying impact test at −20 °C.

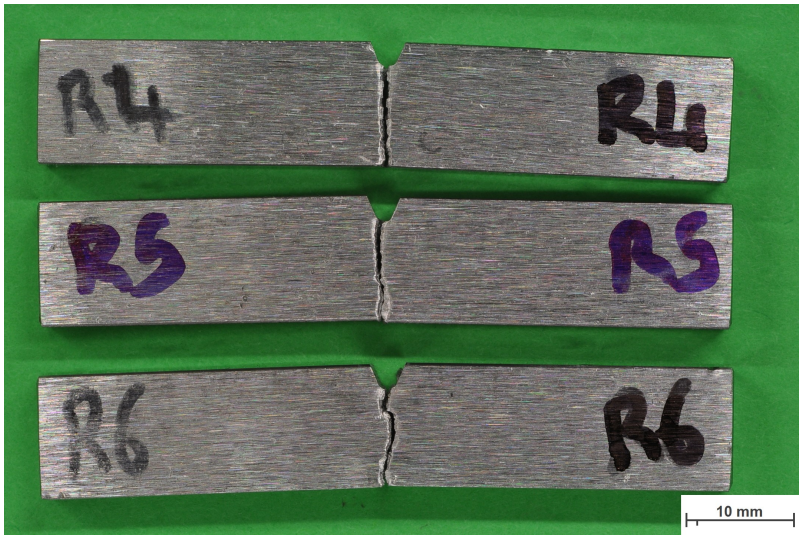

Figure A2: Butt weld as welded Charpy V-notch samples after applying impact test at −40 °C.

Figure A3: Butt weld EBLPWHT (T) Charpy V-notch samples after applying impact test at −20 °C.

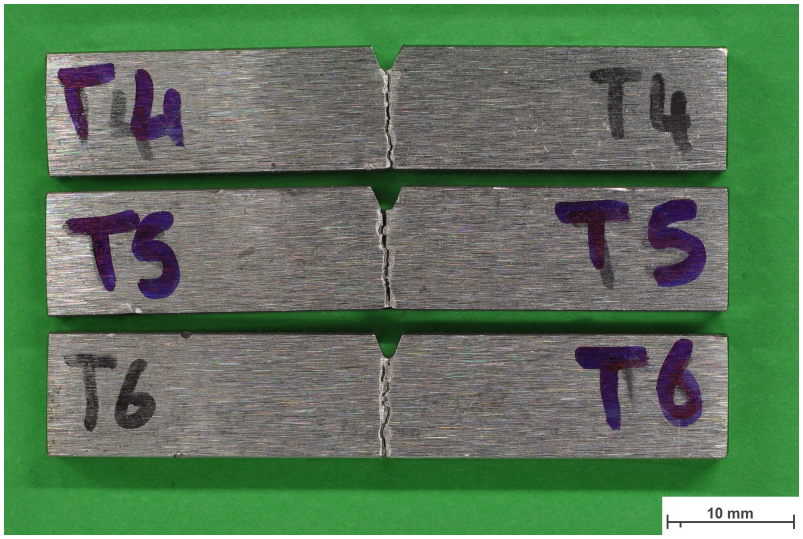

Figure A4: Butt weld EBLPWHT (T) Charpy V-notch samples after applying impact test at −40 °C.

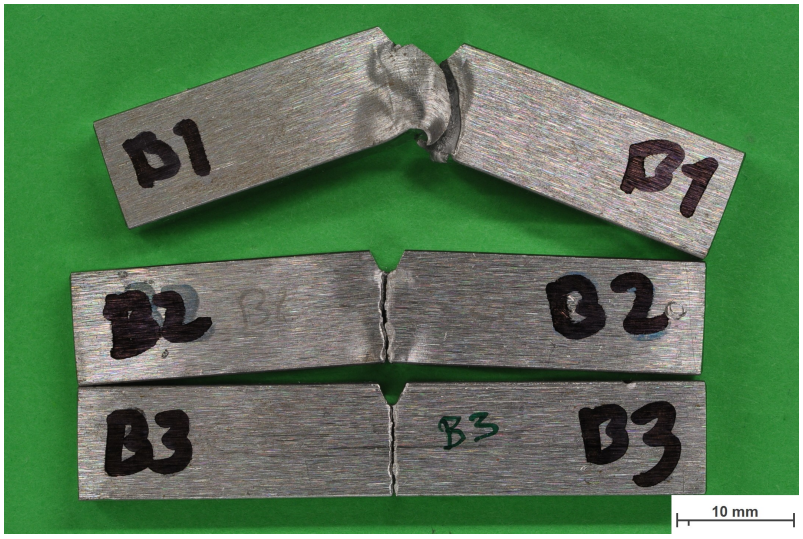

Figure A5: Butt weld EBLPWHT (B) Charpy V-notch samples after applying impact test at −20 °C.

Figure A6: Butt weld EBLPWHT (B) Charpy V-notch samples after applying impact test at −40 °C.

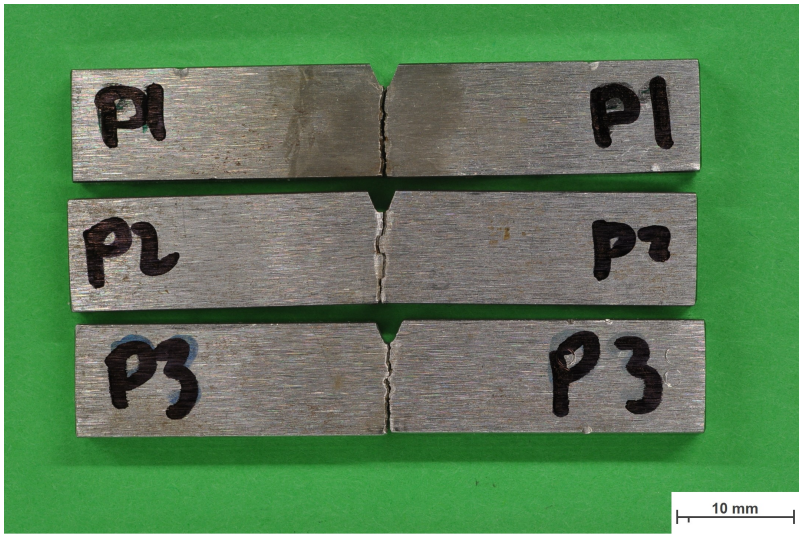

Figure A7: Butt weld EBLPWHT (P) Charpy V-notch samples after applying impact test at −20 °C.

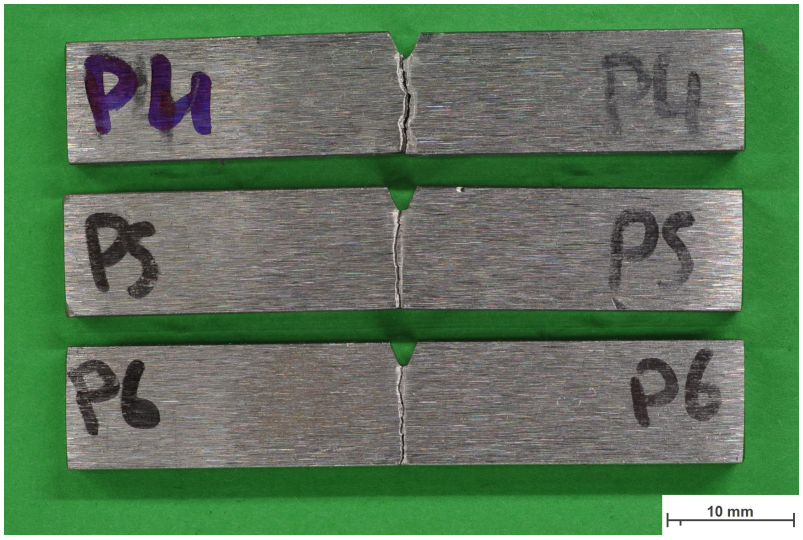

Figure A8: Butt weld EBLPWHT (P) Charpy V-notch samples after applying impact test at −40 °C.

Figure A9: Butt weld Gleeble-PWHT Charpy V-notch samples after applying impact test at −20 °C.

Figure A10: Butt weld Gleeble-PWHT Charpy V-notch samples after applying impact test at −40 °C.

A2 Tensile test

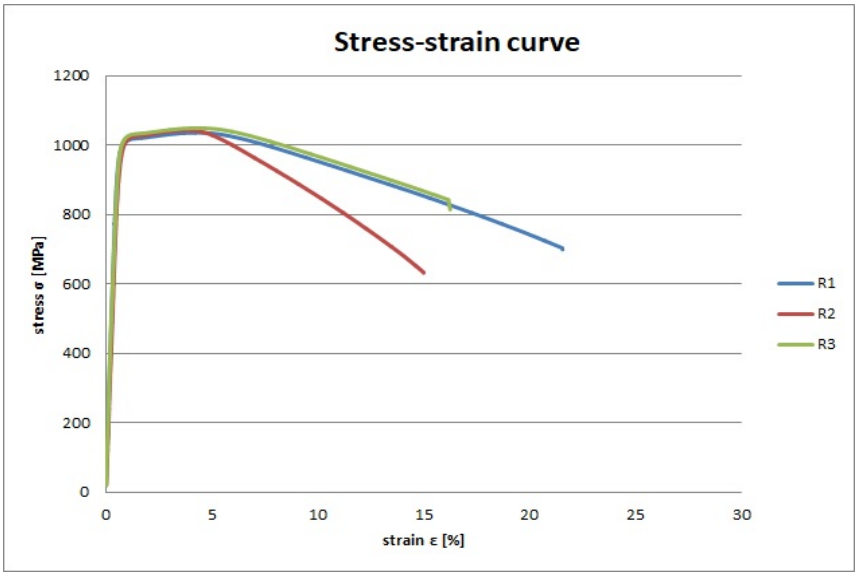

Figure A11: Measured stress-strain curve of the butt weld sample as-welded.

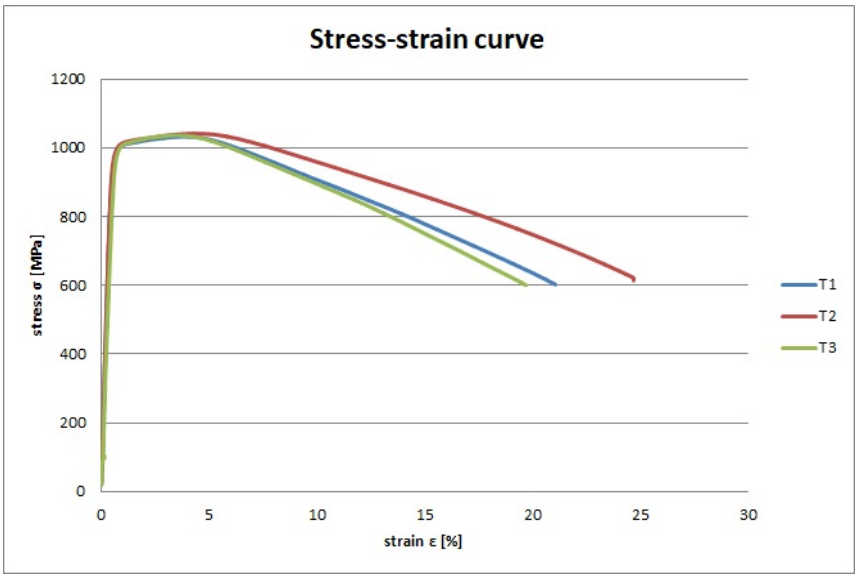

Figure A12: Measured stress-strain curve of the butt weld sample EBLPWHT (T).

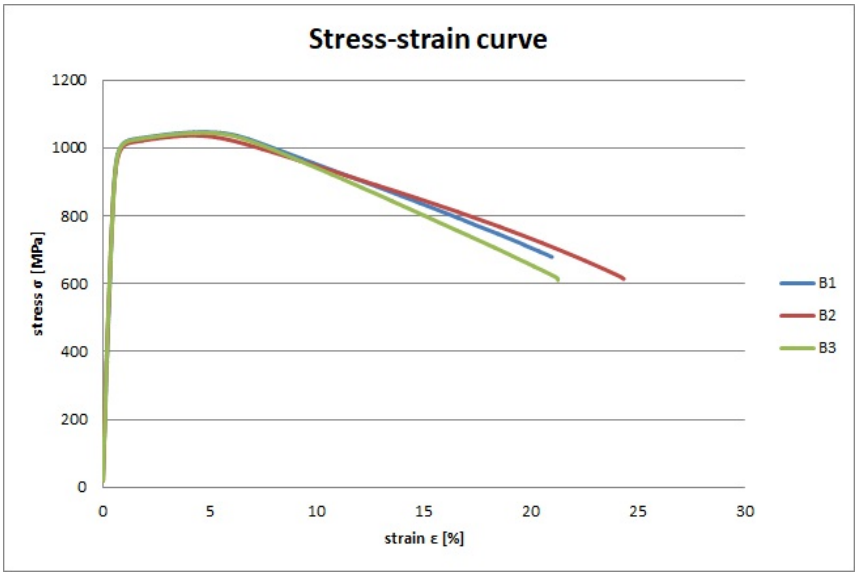

Figure A13: Measured stress-strain curve of the butt weld sample EBLPWHT (B).

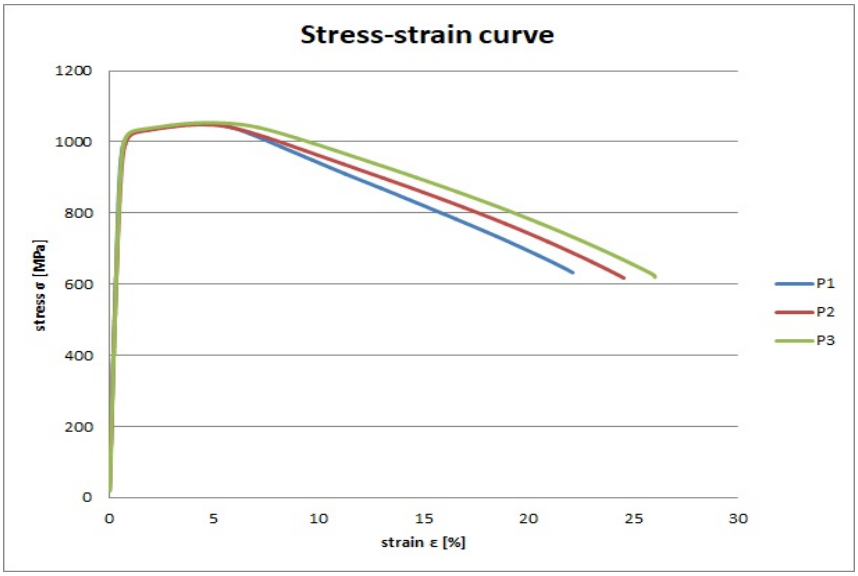

Figure A14: Measured stress-strain curve of the butt weld sample EBLPWHT (P).

Table A5: Measured tensile strength values for the butt weld samples as well as average tensile strength of the tested samples,values in (MPa)

	tensile strength	average tensile strength
As-welded (R)	1021, 1021, 1020	1020.66 ± 0.4
EBLPWHT (T)	1032, 1041, 1036	1036.33 ± 3.6
EBLPWHT (B)	1047, 1037, 1044	1042.66 ± 4.1
EBLPWHT (P)	1051, 1049, 1054	1051.33 ± 2.0

Table A6: Measured yield strength values for the butt weld samples as well as average yield strength of the tested samples,values in (MPa)

	yield strength	average yield strength
As-welded (R)	993, 993, 992	993 ± 0.8
EBLPWHT (T)	971, 976, 995	980 ± 10.0
EBLPWHT (B)	997, 956, 969	967 ± 8.6
EBLPWHT (P)	988, 980, 987	985 ± 3.4

Table A7: Measured fracture elongation values for the butt weld samples as well as the average fracture elongation of the tested samples,values in (%)

	fracture Elongation	average fracture Elongation
As-welded (R)	21, 14, 15	17 ± 2.8
EBLPWHT (T)	20, 24, 19	21 ± 2.1
EBLPWHT (B)	20, 24, 21	21 ± 1.5
EBLPWHT (P)	21, 24, 25	23 ± 1.6